Describing Binary Mixture Diffusion in Carbon Nanotubes with the Maxwell−Stefan Equations. An Investigation Using Molecular Dynamics Simulations

R. Krishna* and J. M. van Baten

Van't Hoff Institute for Molecular Sciences, University of Amsterdam, Nieuwe Achtergracht 166, 1018 WV Amsterdam, The Netherlands

Adsorption and diffusion of pure components and binary mixtures containing methane, ethane, propane, *n*-butane, isobutane, and hydrogen at 300 K in a variety of configurations of carbon nanotubes (CNTs) have been investigated using configurational-bias Monte Carlo (CBMC) simulations and molecular dynamics (MD) simulations. Both self-diffusivities, $D_{i,\mathrm{self}}$, and the Maxwell−Stefan (MS) diffusivities, $Đ_i$, were determined for a variety of molecular loadings Θ, approaching saturation limits. For comparison purposes, self-diffusivities were also determined in pure fluids of varying densities using MD. At low loadings Θ, the $D_{i,\mathrm{self}}$ correspond to the value for low-density gases. With increasing loadings, however, the $D_{i,\mathrm{self}}$ in CNTs are slightly higher than the values in fluids when compared at the same molecular density. In CNTs, the $D_{i,\mathrm{self}}$ is significantly smaller in magnitude than the MS diffusivity $Đ_i$, signifying strong correlations between molecular jumps along the tube. Consequently, for mixture diffusion, the component self-diffusivities are close together. MD simulations of binary-mixture diffusion demonstrate that the mixture-diffusion characteristics can be estimated with good accuracy from the pure-component diffusion parameters using the MS diffusion formulation. In the estimation procedure, the binary-exchange parameter $Đ_{12}$ is estimated from the pure-component self-exchange coefficients $Đ_{11}$ and $Đ_{22}$ using the interpolation scheme suggested earlier for transport in zeolites (Skoulidas et al. *Langmuir* **2003**, *19*, 7977).

1. Introduction

Carbon nanotubes (CNTs) consist of a graphite sheet rolled up into a cylinder with a diameter on the order of a nanometer and a length of several micrometers; see Figure 1 parts a and b. Since their discovery in 1991 by Iijima[1] as nested structures of concentric shells, carbon multiwall and single-wall nanotubes have been synthesized using a variety of techniques.[2,3] CNTs possess potential as a stable and effective adsorbent material for hydrogen storage and for separation of a variety of mixtures,[4] including nitrogen and oxygen,[5,6] alkanes,[7,8] enantiomers,[9] carbon monoxide and hydrogen,[10] hydrogen isotopes,[11] and alkanes and hydrogen.[12,13]

In recent years, molecular simulations techniques, such as (configurational-bias) Monte Carlo (CBMC) and molecular dynamics (MD), have proved to be potent tools for exploring the adsorption and diffusion characteristics of a variety of molecules in CNTs, and a large number of publications on this subject have emerged from a number of research groups including those of Sholl,[11−18] Sinnott,[2,7,19−22] Sandler,[5,6,8,23] Bhatia,[17,24] Keil,[25−30] Seaton,[31] Garberoglio,[32,33] Sheintuch,[34,35] Jiang,[36] Nicholson,[37] and Nitta.[10]

Diffusion in CNTs has been shown to be much more rapid than in other nanoporous structures such as zeolites.[12−14,38] While a majority of the published studies relate to single-component adsorption and diffusion, a few papers have also addressed adsorption[7,8] and diffusion[12,13] of mixtures.

From the viewpoint of design of separation devices such as CNT membranes for separation of mixtures, it is essential to use the proper set of diffusion equations. Chen and Sholl[12] have adopted the Onsager formulation based on irreversible thermodynamics, closely following the treatment of Skoulidas et al.[39] for binary diffusion through zeolite membranes. The matrix of Onsager coefficients [*L*] describing binary diffusion was obtained by fitting of the MD simulation data for binary diffusion.

In recent years, the Maxwell−Stefan (MS) diffusion formulation has been used with considerable success to describe mixture diffusion in zeolites.[40−47] Adopting this formulation for one-dimensional (1D) transport within a CNT tube, the fluxes $\mathbf{N}_i$ of species *i*, expressed in molecules per second per square meter of cross-sectional area, can be related to the chemical potential gradients by

$$-\frac{1}{A_{\mathrm{CNT}}}\frac{\Theta_i}{k_{\mathrm{B}}T}\nabla\mu_i=\sum_{\substack{j=1\\ j\neq 1}}^{n}\frac{\Theta_j\mathbf{N}_i-\Theta_i\mathbf{N}_j}{\Theta_{j,\mathrm{sat}}Đ_{ij}}+\frac{\mathbf{N}_i}{Đ_i};\quad i=1,\ldots,n \tag{1}$$

In eq 1, Θ_i is the loading within the CNT expressed in molecules per unit tube length, $\Theta_{i,\mathrm{sat}}$ represents the saturation loading of species *i*, *n* is the total number of diffusing species, and k_{B} is the Boltzmann constant. Equation 1 *defines* two types of MS diffusivities: $Đ_i$ and $Đ_{ij}$. If we have only a single sorbed component, then only one $Đ_i$ is needed, and in this case, $Đ_i$ is equivalent to the "corrected" diffusivity.[48] The binary-exchange coefficients $Đ_{ij}$ reflect *correlation* effects in mixture diffusion.[49] For mixture diffusion, the correlation effects tend to slow the more-mobile species and speed up the relatively sluggish ones. A lower value of the exchange coefficient $Đ_{ij}$ implies a *stronger* correlation effect. For two-component mixture diffusion within MFI zeolite, a logarithmic interpolation formula has been suggested,[43]

$$\Theta_{2,\mathrm{sat}}Đ_{12}=[\Theta_{2,\mathrm{sat}}Đ_{11}]^{\Theta_1/(\Theta_1+\Theta_2)}[\Theta_{1,\mathrm{sat}}Đ_{22}]^{\Theta_2/(\Theta_1+\Theta_2)}=\Theta_{1,\mathrm{sat}}Đ_{21} \tag{2}$$

for estimating the binary-exchange parameter $Đ_{12}$ from informa-

* Corresponding author. Fax: +31 20 5255604. E-mail: r.krishna@uva.nl.

10.1021/ie051126d CCC: $33.50
Published on Web 02/11/2006

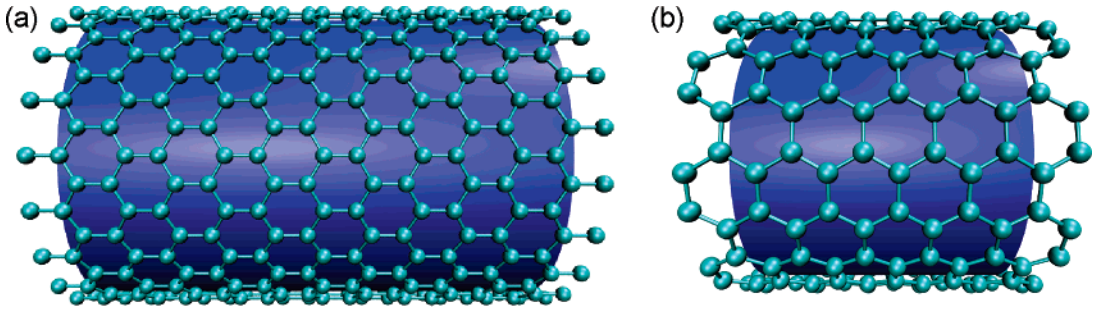

Figure 1. Two configurations of CNTs, (a) zigzag, CNT (20, 0), and (b) armchair, CNT (10, 10).

Table 1. MD Simulation Campaigns with Various Alkanes in Various CNT Topologies[a]

CNT	*n*	components	campaign
zigzag (20,0)	1	C1, C2, C3, nC4, iC4	pure, varying Θ
	2	C1/C2, C1/C3, C1/nC4, C1/iC4	50−50 mixtures, varying Θ
	2	C1/C2	varying x_i, keeping Θ constant
armchair (10,10)	1	C1, H2	pure, varying Θ
	2	C1/H2	50−50 mixtures, varying Θ
	2	C1/H2	varying x_i, keeping Θ constant
zigzag (17,0)	1	C1	pure, varying Θ
zigzag (15,0)	1	C1	pure, varying Θ
zigzag (11,0)	1	C1	pure, varying Θ

[a] Each simulation was run for 5 ns, and the MSD data were fitted for the 0.5−5 ns time range.

Table 2. Lennard-Jones Parameters[a]

site	σ	(ϵ/k_B)
H2	0.296	34.2
C(wall)	0.34	28

[a] The units of σ are nm, and those of (ϵ/k_B) are K.

Table 3. Dimensions (in nm) of CNTs Used in the Simulations.

CNT	diameter[a]	unit cell length
zigzag (20,0)	1.5674	0.426
zigzag (17,0)	1.3328	0.426
zigzag (15,0)	1.1765	0.426
zigzag (11,0)	0.8641	0.426
armchair (10,10)	1.3579	0.246

[a] The diameter represents the center-to-center distance of C atoms on the CNT wall.

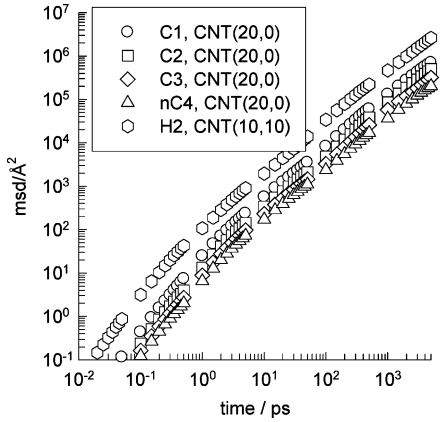

Figure 2. Typical MSD data for C1, C2, C3, and nC4 in CNT (20, 0) at a loading of 1.956 molecules/nm. Also shown is MSD data for H2 in CNT (10, 10) at a loading of 2.25 molecules/nm. Diffusivities were determined by linear regression in the time range of 500−5000 ps.

tion on the pure-component *self*-exchange coefficients $Đ_{11}$ and $Đ_{22}$. The self-exchange diffusivities $Đ_{ii}$ are determined from information on MS *and* self-diffusivities.[43]

An important advantage of the MS formulation is that mixture diffusion can be estimated on the basis of pure-component diffusion and adsorption data. The major objective of the present communication is to examine the extent to which the MS theory is successful in describing mixture diffusion in CNTs. For this purpose, we use MD simulations to study diffusion of both pure components (methane (C1), ethane (C2), propane (C3), *n*-butane (nC4), isobutane (iC4), and hydrogen (H2)) and binary mixtures (C1−C2, C1−C3, C1−nC4, C1−iC4, and C1−H2) for a variety of loadings in CNTs of both zigzag ((20, 0), (17, 0), (15, 0), and (11, 0)) and armchair (10, 10) configurations. Additionally, CBMC simulations were carried out to determine the sorption isotherms for pure components and binary mixtures; this information is required for interpretation of the diffusion data.

We aim to show that correlation effects are very strong for diffusion in CNTs, much stronger than for diffusion within zeolites. Furthermore, we aim to show that such strong correlation effects have a significant impact on mixture diffusion behavior that has hitherto not been fully appreciated. The second major objective is to test the applicability of the interpolation formula (eq 2) for capturing correlation effects in binary-mixture diffusion.

2. CBMC and MD Simulation Methodologies

Simulations have been carried out for diffusion, and adsorption, of pure components ($n = 1$) and binary ($n = 2$) mixtures containing C1, C2, C3, nC4, iC4, and H2 in both zigzag and armchair CNT configurations; the various campaigns are specified in Table 1. We use the united atom model. The force field for the alkanes are the same as those reported by Dubbeldam et al.[50] We consider the CH_x groups as single, chargeless interaction centers with their own effective potentials. The beads in the chain are connected by harmonic bonding potentials. A harmonic cosine bending potential models the bond bending between three neighboring beads; a Ryckaert−Bellemans potential controls the torsion angle. The beads in a chain separated by more than three bonds interact with each other through a Lennard-Jones potential. The force field for the CNT wall and H2 are given in Table 2. The force field for the C wall is the same as that developed for graphite.[14,16,27,51] The force field for H2 is taken from the literature.[52] The force fields for alkanes have been given in detail in an earlier publication.[50] The solid−fluid potentials were derived from the Lorentz−Berthelot combining rules $\sigma_{ij} = (\sigma_i + \sigma_j)/2$; $\epsilon_{ij} = \sqrt{\epsilon_i \epsilon_j}$. The Lennard-Jones potentials are shifted and cut at 1.2 nm. We assume that the nanotubes are completely rigid, with all carbon atoms fixed in their ideal lattice positions. The recent study of Chen et al.[18] has confirmed that the accounting for the flexibility for the CNT tube wall has only a small influence on the diffusivities when the pressure is above ~1 bar.

Pure-component adsorption isotherms were determined using configurational-bias Monte Carlo (CBMC) simulations follow-

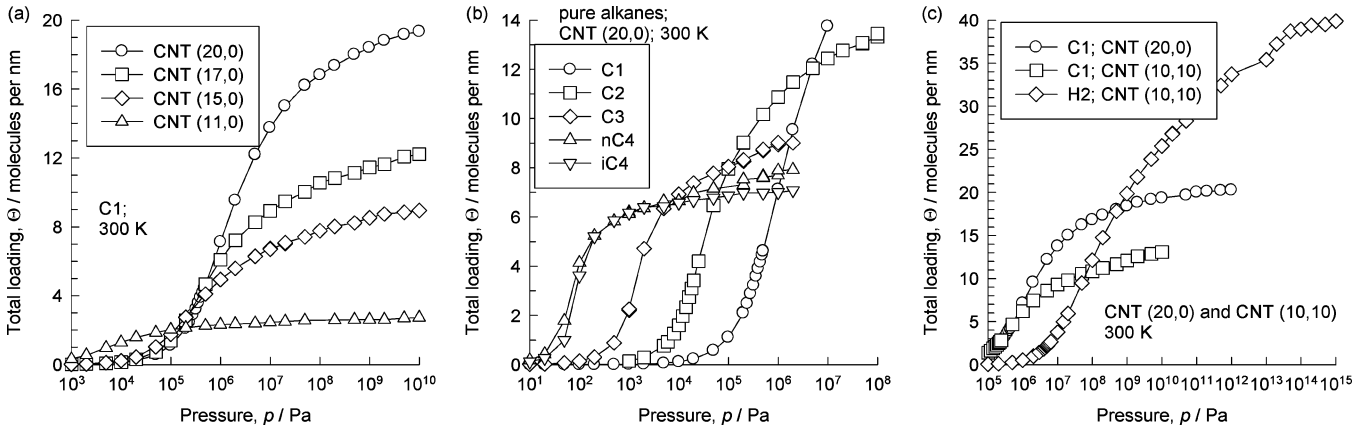

Figure 3. CBMC simulated isotherms (a) for C1 in CNT (11, 0), CNT (15, 0), CNT (17, 0), and CNT (20, 0); (b) for C1, C2, C3, nC4, and iC4 in CNT (20, 0); and (c) for C1 and H2 in CNT (10, 10).

Table 4. Pure-Component Saturation Capacities and Diffusion Data[a]

				parameters describing self-exchange, defined by eq 9		Reed−Ehrlich model parameters in eq 10 and (11)	
component and CNT	saturation capacity, $\Theta_{i,sat}$	inflection, Θ_{infl}	$Đ_i(0)$	a	b	γ	δ
C1 in CNT (20, 0)	20	2	7500	0.0006	0.037	0.04	3.3
C1 in CNT (17, 0)	13	2	7500	0.0005	0.032	0.04	3.2
C1 in CNT (15, 0)	10	2	7500	0.0003	0.03	0.04	2.5
C1 in CNT (11, 0)	2.75	2	7500	0.0002	0.025	0.3	0.5
C2 in CNT (20, 0)	14	2	2500	0.0012	0.03	0.17	3.0
C3 in CNT (20, 0)	9	2	950	0.0032	0.023	0.7	2.0
nC4 in CNT (20, 0)	8	2	720	0.0033	0.0282	0.9	1.5
iC4 in CNT (20, 0)	7	2	720	0.0033	0.024	0.9	1.5
C1 in CNT (10, 10)	13	2.2	7500	0.00035	0.028	0.35	2.5
H2 in CNT (10, 10)	40	2.2	9200	0.0005	0.032	0.2	2.6

[a] The data on $\Theta_{i,sat}$ and Θ_{infl} are in molecules per nm. The zero-loading diffusivities $Đ_i(0)$ are in units of 10^{-8} m^2 s^{-1}.

ing the procedure described in earlier publications[50,53,54] and a simulation box consisting of a single CNT, with the length of 36 unit cells; the unit-cell dimensions for the various CNTs simulated are specified in Table 3.

Diffusion is simulated using Newton's equations of motion until the system properties, on average, no longer change in time. The Verlet algorithm is used for time integration. The energy drift of the entire system is monitored to ensure that the time steps taken were not too large. A time step of 5 fs was used in all simulations. For each simulation, *initializing* CBMC moves are used to place the molecules in the domain, minimizing the energy. Next, follows an *equilibration* stage. Like the initialization stage, this consists of CBMC moves, but now using velocity scaling; at each cycle, all adsorbent pseudo-atom velocities are scaled to match the specified temperature. After a fixed number of initialization and equilibrium steps, the MD simulation *production* cycles start. For every cycle, the statistics for determining the mean square displacements (MSDs) are updated. The MSDs are determined for time intervals ranging from 2 fs to 1 ns. To do this, an order-N algorithm, as detailed in Chapter 4 of Frenkel and Smit,[55] is implemented. The Nosé−Hoover thermostat is applied to all the diffusing particles, ensuring that the dynamical properties correspond to that of an NVE ensemble.[55]

The MD simulations were carried out for a variety of molecular loadings within the CNT. For 1D transport of molecules within CNTs of different configurations, it is convenient to express the loadings in terms of molecules per tube length, Θ_i. This also makes it more convenient to compare with transport within zeolites having 1D channels, e.g., AFI, MTW, MOR, FER, and TON. For zigzag CNTs, a minimum tube length of 36 unit cells was used, and for the armchair configuration, a minimum tube length of 72 unit cells was used. To get accurate statistics for diffusivity determinations at low loadings, a minimum number of 40 molecules was used, resulting in simulation boxes with tube lengths of a few hundred unit cells for low loadings. All simulations were carried out on clusters of PCs equipped with Intel Xeon processors running at 3.4 GHz on the Linux operating system. Each MD simulation, for a specified loading, was run for 72 h, determined to be long enough to obtain reliable statistics for determination of the diffusivities.

The self-diffusivities, $D_{i,self}$, in single-component and binary mixtures were computed by analyzing the mean square displacement of each component:

$$D_{i,\text{self}} = \frac{1}{2N_i}\lim_{\Delta t\to\infty}\frac{1}{\Delta t}\left[\left(\sum_{l=1}^{N_i}(\mathbf{r}_{l,i}(t+\Delta t)-\mathbf{r}_{l,i}(t))^2\right)\right] \qquad (3)$$

In this expression, N_i represents the number of molecules of species i and $\mathbf{r}_{l,i}(t)$ is the position of molecule l of species i at any time t. Typical MSDs are shown in Figure 2. For short times, the MSDs vary as t^2, suggesting ballistic motion of molecules. Diffusive motion is realized when $t > 100$ ps. The diffusivities were determined by linear regression of the MSD data in the time interval 500−5000 ps.

In the work of Chen and Sholl[12] on diffusion of CH_4−H_2 binary mixture in CNT, the Onsager matrix $[L]$, defined by $(\mathbf{N}) = [L](\nabla\mu)$, was determined from the MSDs. From the viewpoint of the application of the MS diffusion formulation, we find it

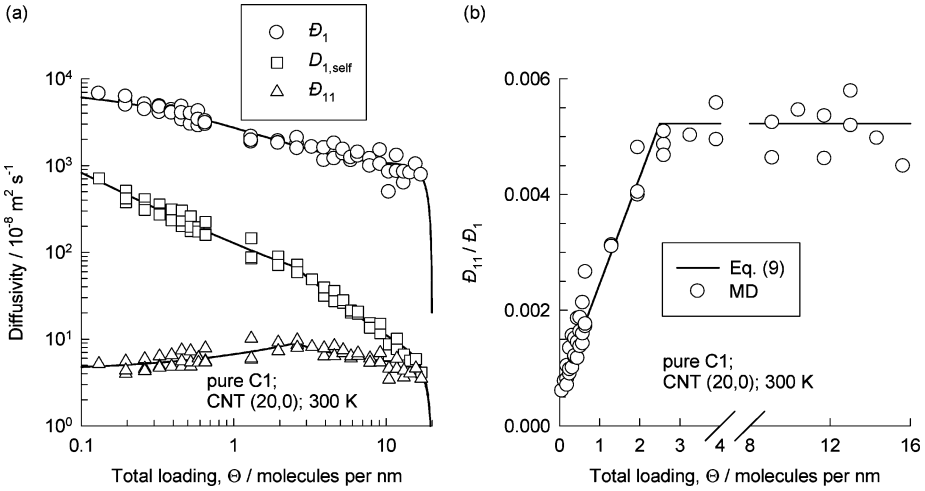

Figure 4. Diffusion of C1 in CNT (20, 0) at 300 K. The MD simulation results (open symbols) for (a) $D_{i,\mathrm{self}}$, $Đ_i$, $Đ_{ii}$ and (b) $Đ_{ii}/Đ_i$. The continuous solids represent calculations using eqs 9−13 with parameters specified in Table 4.

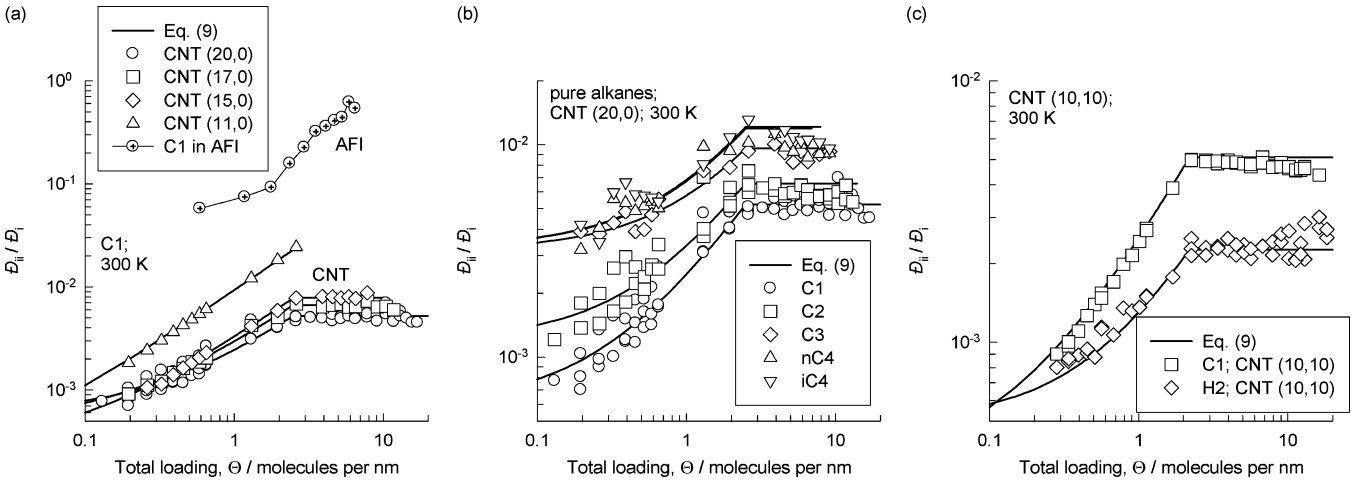

Figure 5. Ratio of self-exchange to MS diffusivity, $Đ_{ii}/Đ_i$ from MD simulations (open symbols) (a) for C1 in CNT (11, 0), CNT (15, 0), CNT (17, 0), and CNT (20, 0); (b) for C1, C2, C3, nC4, and iC4 in CNT (20, 0); and (c) for C1 and H2 in CNT (10, 10). The continuous solids represent calculations using eq 9 with parameters specified in Table 4. Also shown in (a) are the values of $Đ_{ii}/Đ_i$ for C1 in AFI at 300 K.

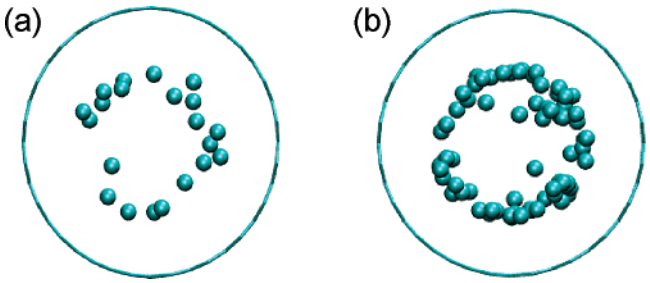

Figure 6. Snapshots of location of methane molecules in CNT (20, 20) at loadings of (a) $\Theta_i = 1.11$ and (b) $\Theta_i = 4.62$ molecules/nm.

more convenient to define a matrix [Δ],

$$\mathbf{N}_i = -\frac{1}{A_{\mathrm{CNT}}k_{\mathrm{B}}T}\Theta_i\sum_{j=1}^{2}\Delta_{ij}\nabla\mu_j; \quad i = 1, 2 \tag{4}$$

and determine the elements of this matrix from

$$\Delta_{ij} = \frac{1}{2N_i}\lim_{\Delta t\to\infty}\frac{1}{\Delta t}[(\sum_{l=1}^{N_i}(\mathbf{r}_{l,i}(t+\Delta t) - \mathbf{r}_{l,i}(t)))(\sum_{k=1}^{N_j}(\mathbf{r}_{k,j}(t+\Delta t) - \mathbf{r}_{k,j}(t)))] \tag{5}$$

In this expression, N_i and N_j represent the number of molecules of species i and j, respectively, and $\mathbf{r}_{l,i}(t)$ is the position of molecule l of species i at any time t. From the definition $\Theta_i = N_i A_{\mathrm{CNT}}/V$, where V is the volume of the simulation box, we see that $\rho\Theta_i\Delta_{ij} = L_{ij}k_{\mathrm{B}}T$, and therefore, the Onsager reciprocal relations $L_{ij} = L_{ji}$ yields

$$\Theta_i\Delta_{ij} = \Theta_j\Delta_{ji} \tag{6}$$

For single-component diffusion, $n = 1$, Δ_{11} can be identified with the MS, or "corrected", diffusivity $Đ_1$.

3. Results for Single-Component Sorption and Diffusion

CBMC simulation results for pure-component sorption of C1, C2, C3, nC4, iC4, and H2 in various CNT configurations are summarized in Figure 3. From these isotherms, we determine the saturation capacities $\Theta_{i,\mathrm{sat}}$ as listed in Table 4 for each species i in a particular CNT configuration.

Consider diffusion of C1 in CNT (20, 0); the MD simulation results for self-diffusivity $D_{1,\mathrm{self}}$ and the MS diffusivity D_1 are shown in Figure 4a for a range of molecular loadings approaching saturation limits. Also shown is the self-exchange

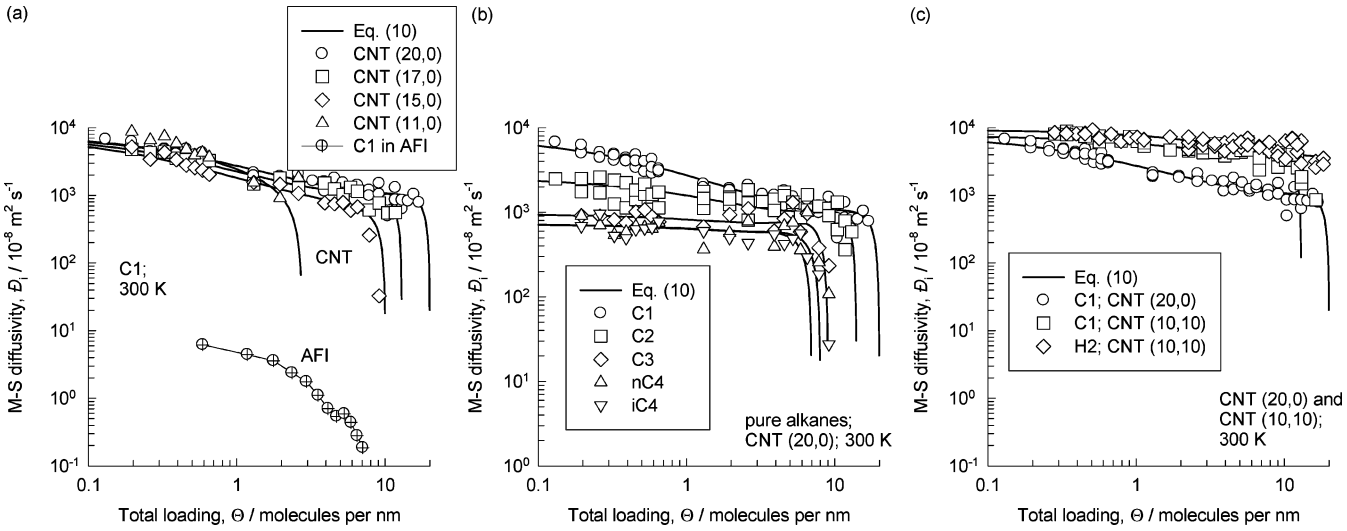

Figure 7. M-S diffusivity, $Đ_i$, from MD simulations (open symbols) (a) for C1 in CNT (11, 0), CNT (15, 0), CNT (17, 0), and CNT (20, 0); (b) for C1, C2, C3, nC4, and iC4 in CNT (20, 0); and (c) for C1 and H2 in CNT (10, 10). The continuous solids represent calculations using eq 9 with parameters specified in Table 4. Also shown in (a) are the values of $Đ_i$ for C1 in AFI at 300 K.

coefficient $Đ_{11}$ calculated from

$$Đ_{11} = \frac{\theta}{\dfrac{1}{D_{1,\text{self}}} - \dfrac{1}{Đ_1}} \tag{7}$$

where θ is the fractional occupancy:

$$\theta = \frac{\Theta}{\Theta_{\text{sat}}} \tag{8}$$

The ratio of the self-exchange coefficient to the MS diffusivity, $Đ_{11}/Đ_i$, shown in Figure 4b, increases linearly with loading until a loading $\Theta_{\text{infl}} = 2$ molecules/nm is reached. For values $\Theta \geq \Theta_{\text{infl}}$, $Đ_{11}/Đ_i$ is practically loading-independent. The self-exchange data were correlated in the form

$$\begin{aligned} \frac{Đ_{11}}{Đ_1} &= a + b\theta \quad \text{for } \Theta < \Theta_{\text{infl}} \\ \frac{Đ_{11}}{Đ_1} &= b\frac{\Theta_{\text{infl}}}{\Theta_{\text{sat}}} \quad \text{for } \Theta \geq \Theta_{\text{infl}} \end{aligned} \tag{9}$$

and the values of the fitted parameters a and b are given in Table 4. Snapshots obtained from CBMC simulations, showing the siting of methane molecules in CNT (20, 20) at loadings of $\Theta = 1.11$ and $\Theta = 4.62$ molecules/nm, are shown in Figure 6 parts a and b. From examination of these and several other snapshots for all molecule−CNT combinations, it appears that, for $\Theta > \Theta_{\text{infl}}$, there is a distinct layer of adsorbed molecules concentric to the CNT tube, whereas for $\Theta < \Theta_{\text{infl}}$, the molecules appear to be randomly distributed inside the inner core, indicative of gaslike motion inside the tube. Equation 9 was found to be a good representation for all molecule−CNT combinations studied in this work; see Figure 5. The values of $Đ_{11}/Đ_1$ in CNTs are about 2 orders of magnitude lower than those in zeolites;[43,56,57] this can be seen by comparison with the value for C1 in AFI zeolite that has 1D channels of 0.73 nm size (the simulation methodology used for AFI is identical to that employed in our earlier work on diffusion in 1D MOR channels[46]); see Figure 5a. As a consequence, correlation effects on mixture diffusion are much stronger in CNTs than in zeolites.

For describing the loading dependence of the MS diffusivity, we use the model attributed to Reed and Ehrlich[57,58] that has been applied in the case of zeolite diffusion,[45,46,57] even though a physical justification for employing this for CNTs is not available as yet. In the Reed−Ehrlich model, the presence of neighboring molecules is assumed to influence the jump frequencies by a factor $f = \exp(\delta E/k_B T)$, where δE represents the reduction in the energy barrier for diffusion. This model leads to the following expression for the MS diffusivity as a function of the fractional occupancy,

$$Đ_1 = Đ_1(0)\frac{(1+\epsilon)^{z-1}}{(1+\epsilon/f)^z} \tag{10}$$

where z is the coordination number, representing the maximum number of nearest neighbors; for 1D transport within CNTs, we take $z = 2$. The other parameters are defined as follows (see Krishna et al.[57] for more detailed discussions and derivations):

$$\epsilon = \frac{(\beta - 1 + 2\theta)f}{2(1-\theta)}; \quad \beta = \sqrt{1 - 4\theta(1-\theta)(1-1/f)} \tag{11}$$

The parameters f have been fitted with the occupancy dependence

$$f = \gamma \exp(\delta\theta) \tag{12}$$

The fitted parameters γ and δ for various molecule−CNT combinations are listed in Table 4. Parts a−c of Figure 7 show that the loading dependence of $Đ$ in CNTs is adequately captured by the Reed−Ehrlich model, which must be considered to be an empirical fit at this stage. The MS diffusivities in CNTs are about 2−3 orders of magnitude higher than the value for diffusion in AFI zeolite; see comparison in Figure 7a.

From eqs 9−12, we are able to calculate the self-diffusivity as a function of loading using[59]

$$D_{1,\text{self}} = \frac{1}{\dfrac{1}{Đ_1} + \dfrac{\theta}{Đ_{11}}} \tag{13}$$

Figure 8 demonstrates the good agreement between the MD simulated $D_{1,\text{self}}$ values (open symbols) with calculations fol-

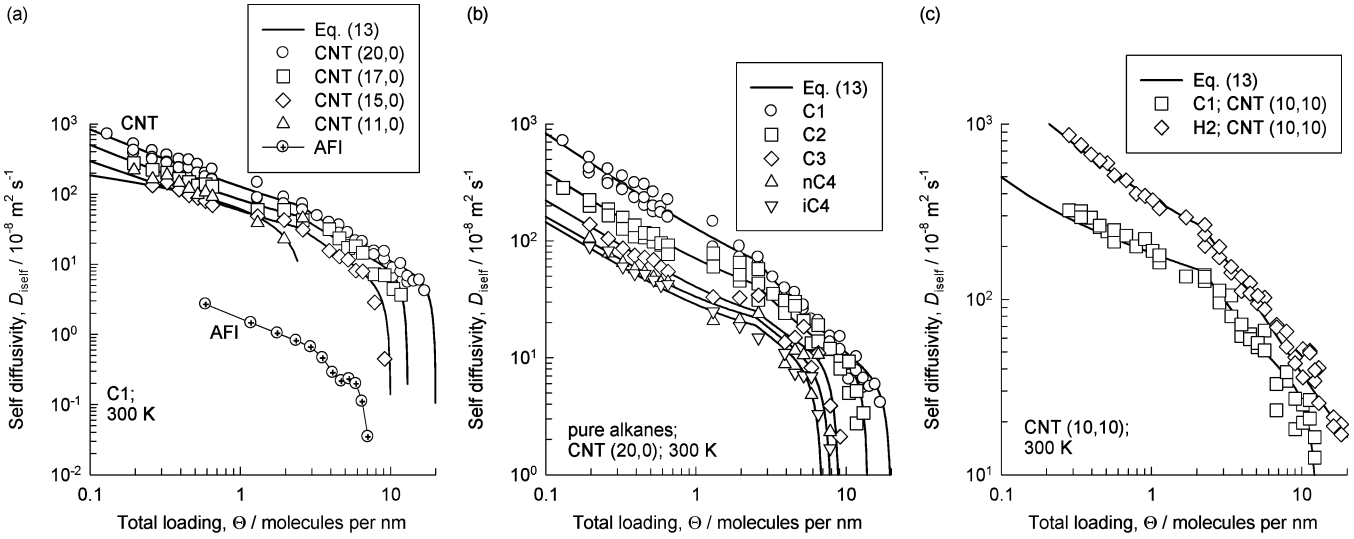

Figure 8. The self-diffusivity, $D_{i,self}$, from MD simulations (open symbols) (a) for C1 in CNT (11, 0), CNT (15, 0), CNT (17, 0), and CNT (20, 0); (b) for C1, C2, C3, nC4, and iC4 in CNT (20, 0); and (c) for C1 and H2 in CNT (10, 10). The continuous solids represent calculations using eqs 9−13 with parameters specified in Table 4.

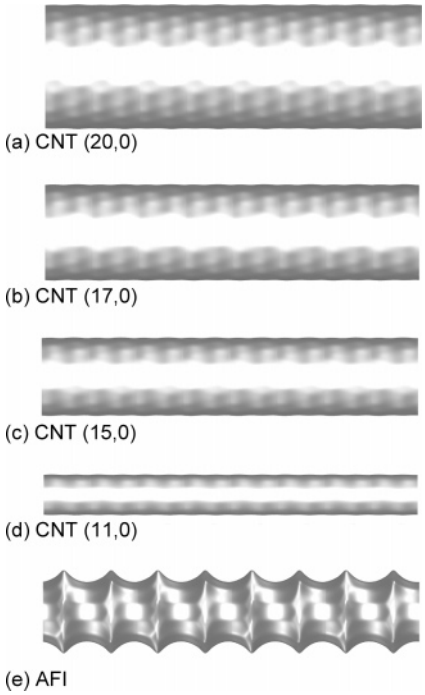

Figure 9. Energy landscapes for (a) CNT (20, 0), (b) CNT (17, 0), (c) CNT (15, 0), (d) (11, 0), and (e) AFI zeolite. The energy landscape diagrams were obtained by using a CH2 cutoff potential of 20 kJ and using the methodology of Clark et al.[60]

lowing eq 13 for the various molecule−CNT combinations. At a loading of 2 molecules/nm, corresponding to Θ_{infl}, there is a slight inflection in the loading dependence of $D_{i,self}$. In Figure 8a, the $D_{i,self}$ values for C1 in various zigzag CNTs are also compared with the corresponding value in 1D channels of AFI zeolite. The self-diffusivities in CNTs are about 2 orders of magnitudes higher than that in AFI.

The explanation for the higher MS and self-diffusivities in CNTs is that the walls of the CNTs are much smoother than in zeolites, as evidenced by the energy landscapes for various CNT zigzag configurations which are compared with that in AFI in Figure 9; see Clark et al.[60] for description of landscape diagrams for zeolites. The same conclusion was reached by Skoulidas et al.[14] by comparing diffusion in CNT with that in MTW zeolite.

To gain further insights into the loading dependence of $D_{i,self}$ in CNTs, we also performed MD simulations to determine self-diffusivities in pure fluids (i.e., without restraining walls) at various molecular loadings; the simulation methodology for pure fluids is that described in an earlier publication.[61] Figure 10 compares the $D_{i,self}$ in CNTs and those in pure fluids where the comparison is made at the same loading expressed in molecules per cubic nanometer. For this purpose, the cross-sectional area of the CNT was taken to be $\pi d^2_{CNT}/4$, where the d_{CNT} values are specified in Table 3; these correspond to the center-to-center distance of the C atoms on the wall. The accuracy of the MD simulations for pure fluids is evidenced by the very good agreement with the experimental data of Greiner-Schmid et al.[62] for C1, C2, and C3; compare the crosses with pluses in Figure 10 parts a−c. At low loadings, there is good agreement between the self-diffusivities in pure fluids and in CNTs, implying that the motion inside the tube is fluid(gas)-like. At higher loadings, the $D_{i,self}$ in CNTs are slightly higher than those in pure fluids. One possible reason for the higher diffusivities in CNTs could be due to the assumption of a rigid wall. Jakobtorweihen et al.[30] have compared diffusivities of C1 in CNT (20, 0) for flexible and rigid walls and shown that the assumption of rigid walls leads to a slightly higher diffusivity value.

4. Results for Binary Mixture Sorption and Diffusion in CNT

First let us consider sorption of a binary mixture of C1 and C2 in CNT (20, 0) at 300 K; CBMC simulations for $p_1 = p_2$ are shown in Figure 11a. At high system pressures, the loading of C2 reaches a maximum and then falls down; this is due to size entropy effects as explained by Jiang et al.;[8] such entropy effects are entirely analogous to that observed for mixture sorption within 1D channels of zeolites.[46,63]

MD simulation results for Δ_{ij} and $D_{i,self}$ for equimolar C1−C2 binary mixture diffusion in CNT (20, 0) for a variety of total mixture loadings $\Theta = \Theta_1 + \Theta_2$ are shown by the symbols in Figure 11b. For estimations of diffusivities in binary mixtures on the basis of pure-component diffusivity data, we combine eqs 1 and 4 to obtain an expression that allows calculation

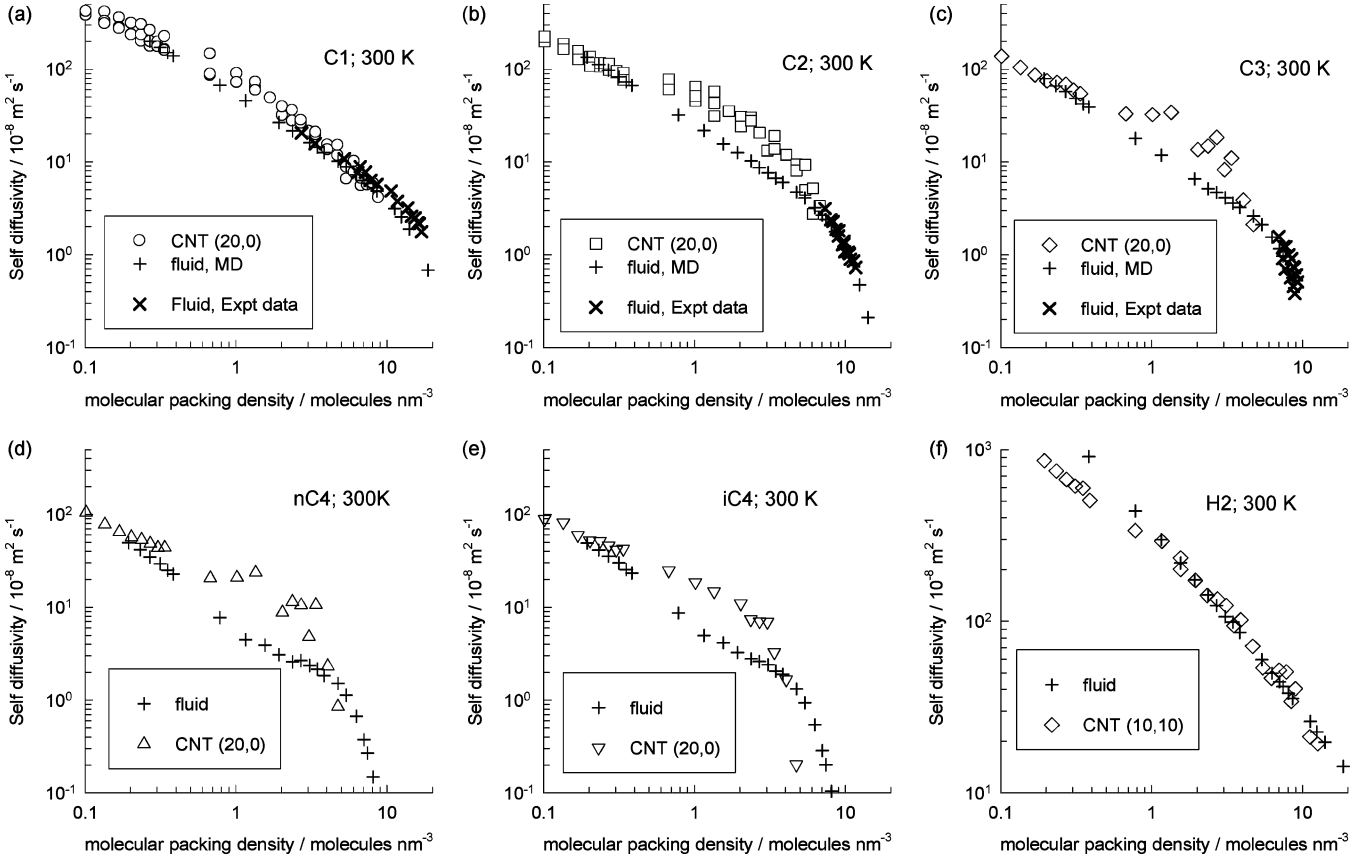

Figure 10. Comparison of the self-diffusivity $D_{i,self}$ in CNT (open symbols) with the value in a pure fluid (pluses), compared at the same molecular loading in the simulation box. For calculation of the volumetric loadings, the cross-sectional area of the CNT was taken to be πd_{CNT}^2, with d_{CNT} values as specified in Table 3. The crosses in (a), (b), and (c) are the experimental data of Greiner-Schmid et al.[62] for temperatures between 294 and 313 K.

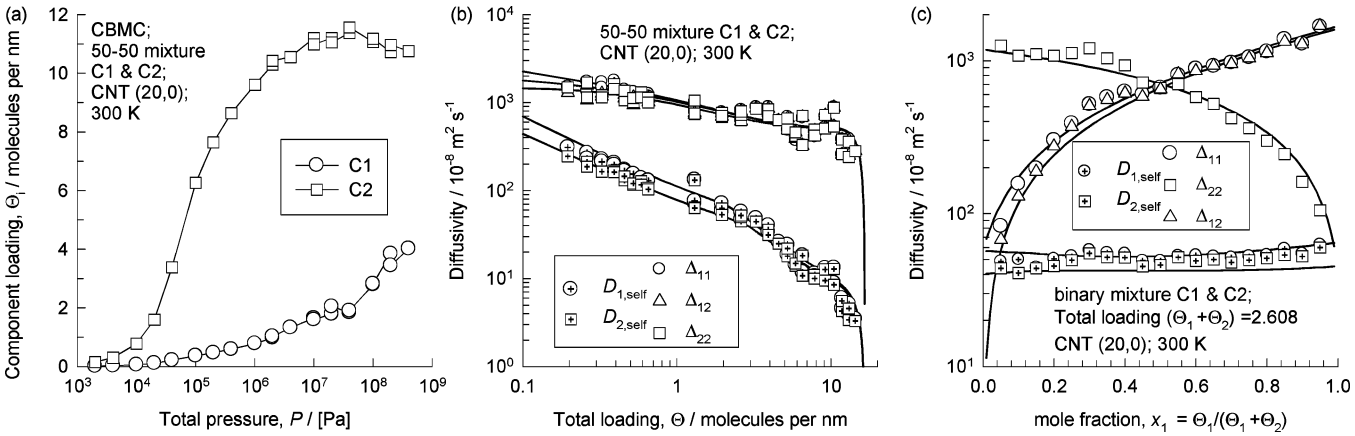

Figure 11. (a) CBMC simulations of sorption of binary mixture of C1 and C2 in CNT (20, 0) at 300 K. (b) MD data (open symbols) for Δ_{ij} and $D_{i,self}$ in 50−50 mixtures of C1 and C2 mixtures in CNT (20, 0) at 300 K. (c) MD data (open symbols) for Δ_{ij} and $D_{i,self}$ as a function of the mole fraction of C1 in C1−C2 mixture at a total loading $\Theta = 2.608$ molecules/nm. The continuous lines in (b) and (c) represent calculations using eqs 14 and 15, with pure-component data as listed in Table 4.

of the elements Δ_{ij}

$$[\Delta] = \begin{bmatrix} 1/Đ_1 + \theta_2/Đ_{12} & -(\Theta_{1,sat}/\Theta_{2,sat})(\theta_1/Đ_{12}) \\ -(\Theta_{2,sat}/\Theta_{1,sat})(\theta_2/Đ_{21}) & 1/Đ_2 + \theta_1/Đ_{21} \end{bmatrix} \tag{14}$$

The self-diffusivities $D_{i,self}$ in the mixture can be calculated from[45]

$$\frac{1}{D_{1,self}} = \frac{1}{Đ_1} + \frac{\theta_1}{Đ_{11}} + \frac{\theta_2}{Đ_{12}}; \quad \frac{1}{D_{2,self}} = \frac{1}{Đ_2} + \frac{\theta_2}{Đ_{22}} + \frac{\theta_1}{Đ_{21}} \tag{15}$$

Following the work of Skoulidas et al.[43] for diffusion in zeolites, we estimate the binary-exchange parameter $Đ_{12}$ from eq 2, with the pure-component self-exchange $Đ_{11}$ and $Đ_{22}$ determined from eq 9 taking the total occupancy in place of component occupancies[43,45]

$$\theta = \theta_1 + \theta_2 = \frac{\Theta_1}{\Theta_{1,sat}} + \frac{\Theta_2}{\Theta_{2,sat}} \tag{16}$$

using the parameters from Table 4. Similarly, the MS diffusivities in the binary mixture, $Đ_1$ and $Đ_2$, are obtained from the Reed−Ehrlich formula (eq 10), using the total occupancy in the mixture. Calculations using eqs 14 and 15 are shown by the continuous solid lines in Figure 11b; the agreement is very good. Because of strong correlation effects, contributions of $1/Đ_1$

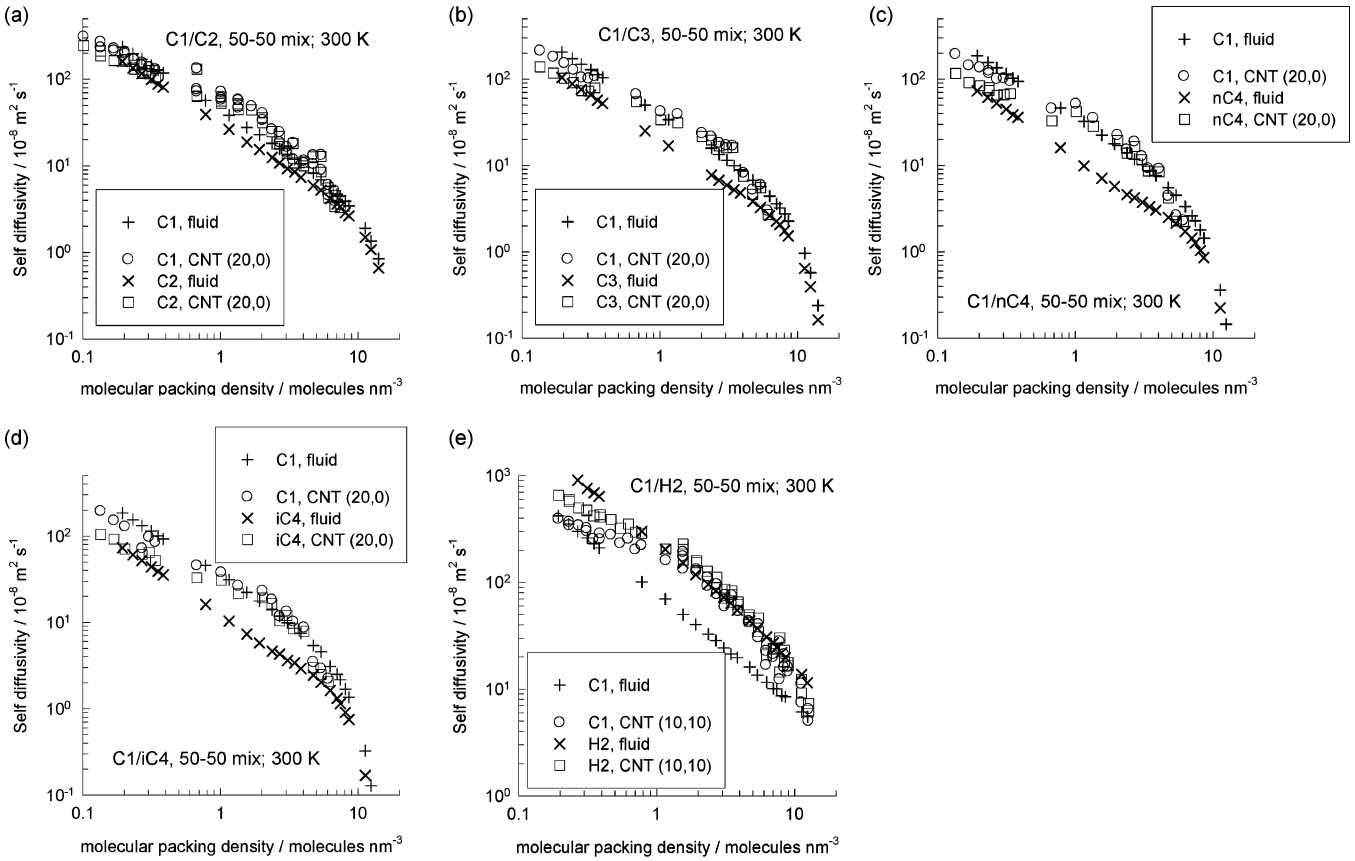

Figure 12. Comparison of the self-diffusivity $D_{i,\text{self}}$ in equimolar binary mixtures of (a) C1−C2, (b) C1−C3, (c) C1−nC4, (d) C1−iC4, and (e) C1−H2 in both CNTs (open symbols) and in fluid mixtures (pluses and crosses) compared at the same molecular loading in the simulation box. For calculation of the volumetric loadings, the cross-sectional area of the CNT was taken to be $\pi d_{\text{CNT}}^2/4$, with d_{CNT} values as specified in Table 3.

and $1/Đ_2$ can be ignored as a first approximation, making the self-diffusivities in the mixture close to one another, $D_{1,\text{self}} \approx D_{2,\text{self}}$ and $\Delta_{11} \approx \Delta_{12} \approx \Delta_{22}$ for an equimolar mixture (i.e., $\Theta_1 = \Theta_2$).

For diffusion in the C1−C2 mixture at a total loading $\Theta = 2.608$ molecules/nm, MD simulations were carried out with varying mole fractions; the data (open symbols) for Δ_{ij} and $D_{i,\text{self}}$ are shown in Figure 11c. Again, the agreement with the estimations from pure-component data using eqs 14 and 15, shown by the continuous solids lines, is very good. Similar good agreement between the predictions of the MS theory and MD simulations was obtained for binary mixtures C1−C3, C1−nC4, and C1−iC4 in CNT (20, 0) and for C1−H2 in CNT (10, 10); these results are presented in graphical form in the Supporting Information accompanying this publication.

Because of strong correlation effects, mixture diffusion in CNTs is quite different from mixture diffusion in fluids, even though there is strong agreement for self-diffusion in *pure* fluids. To stress this point, we also performed MD simulations to determine self-diffusivities in various equimolar C1−C2, C1−C3, C1−nC4, C1−iC4, and C1−H2 fluid mixtures (i.e., without restraining walls); the comparison of results in CNTs and fluids is shown in Figure 12 parts a−e. With increasing molecular packing density, $D_{i,\text{self}}$ in CNTs come closer together. For fluids, the self-diffusivities are much further apart.

Conclusions

We have carried out MD simulations to study diffusion of pure components and binary mixtures containing C1, C2, C3, nC4, iC4, and H2, in a variety of CNT configurations. The following insights and conclusions emerge from this study.

(1) The MS and self-diffusivities of pure components in CNTs are about 2−3 orders of magnitude higher than those for diffusion in 1D channels of zeolites. The higher values in CNTs are due to the smoothness of the CNT walls.

(2) The self-diffusivities of pure components in CNTs are quite close to that in the corresponding pure fluid, and their dependence on the molecular packing density is nearly the same.

(3) Correlation effects are much stronger in CNTs than in zeolites. This is evidenced by the fact that $Đ_{ii}/Đ_i$ are about 1−2 orders of magnitude lower than for zeolites.

(4) The MS formulation, with the interpolation formula (eq 2), is successful in estimating the binary mixture diffusion characteristics in all investigated cases. Since correlation effects are extremely strong in CNTs, the estimation of the exchange parameter $Đ_{12}$ is particularly crucial. Unlike in the case of diffusion in zeolites, contribution of $1/Đ_i$ terms in eq 14 for $[\Delta]$, and in eq 15 for $D_{i,\text{self}}$, can be ignored without loss of accuracy. Consequently, in CNTs, the $D_{i,\text{self}}$ come closer to one another than in either fluids or in zeolites. This aspect has profound implications in the development of separation processes using, say, CNT membranes. Separation selectivities will be *lowered* because of the strong correlation effects. This aspect needs further investigation.

Acknowledgment

The authors acknowledge a TOP subsidy from The Netherlands Foundation for Fundamental Research (NWO-CW) for intensification of reactors. We acknowledge NWO/NCF for provision of high-performance computing resources in terms of PC clusters running on LINUX. We gratefully acknowledge D. Dubbeldam, S. Calero, T. J. H. Vlugt, E. Beerdsen, and B. Smit for providing the CBMC and MD simulation codes.

Supporting Information Available: The Supporting Information including data for binary mixture diffusion in carbon nanotubes that validates the Maxwell−Stefan formulation using molecular dynamics simulations. This document contains the complete set of data on Δ_{ij}, $D_{i,\text{self}}$, $Đ_i$, and $Đ_{ii}$ for each campaign listed in Table 1, in graphical form. This material is available free of charge via the Internet at http://pubs.acs.org.

Notations

A_{CNT} = cross-sectional area of CNT, m^2
a = constant describing self-exchange, dimensionless
b = constant describing self-exchange, dimensionless
d_{CNT} = diameter of CNT tube, m
$D_{i,\text{self}}$ = self-diffusivity, $m^2\ s^{-1}$
$Đ_i$ = Maxwell−Stefan diffusivity of species i, $m^2\ s^{-1}$
$Đ_i(0)$ = zero-loading MS diffusivity of species i, $m^2\ s^{-1}$
$Đ_{ii}$ = self-exchange diffusivity, $m^2\ s^{-1}$
$Đ_{12}$ = binary-exchange diffusivity, $m^2\ s^{-1}$
f = Reed−Ehrlich parameter, dimensionless
k_B = Boltzmann constant, 1.38×10^{-23} J molecule^{-1} K^{-1}
$\mathbf{N}_i$ = molecular flux of species i, molecules $m^{-2}\ s^{-1}$
N_i = number of molecules of species i, molecules
p = system pressure, Pa
p_i = partial pressure of species i, Pa
R = gas constant, 8.314 J mol^{-1} K^{-1}
t = time, s
T = absolute temperature, K
V = volume, m^3
x_i = mole fraction of species i in mixture, dimensionless
z = coordination number, dimensionless

Greek Letters

β = Reed−Ehrlich parameter, dimensionless
γ = parameter describing occupancy dependence of f, dimensionless
δ = parameter describing occupancy dependence of f, dimensionless
$[\Delta]$ = matrix of Maxwell−Stefan diffusivities, $m^2\ s^{-1}$
ϵ = Reed−Ehrlich parameter, dimensionless
θ = fractional occupancy, dimensionless
Θ_i = molecular loading, molecules per unit length of CNT
$\Theta_{i,\text{sat}}$ = saturation loading, molecules per unit length of CNT
μ_i = molar chemical potential, J molecule^{-1}

Subscripts

infl = referring to inflection point in loading
sat = referring to saturation conditions
self = referring to self-diffusivity
i,j = components in mixture

Vector and Matrix Notation

$(\cdot)$ = vector
$[\cdot]$ = square matrix

Literature Cited

(1) Iijima, S. Helical microtubules of graphitic carbon. *Nature* **1991**, *354*, 56−58.

(2) Sinnott, S. B.; Andrews, R. Carbon nanotubes: Synthesis, properties, and applications. *Crit. Rev. Solid State Mater. Sci.* **2001**, *26*, 145−249.

(3) Popov, V. N. Carbon nanotubes: Properties and application. *Mater. Sci. Eng., R* **2004**, *43*, 61−102.

(4) Arab, M.; Picaud, F.; Devel, M.; Ramseyer, C.; Girardet, C. Molecular selectivity due to adsorption properties in nanotubes. *Phys. Rev. B: Condens. Matter* **2004**, *69*, 165401.

(5) Arora, G.; Sandler, S. I. Air separation by single wall carbon nanotubes: Thermodynamics and adsorptive selectivity. *J. Chem. Phys.* **2005**, *123*, 044705.

(6) Jiang, J. W.; Sandler, S. I. Nitrogen and oxygen mixture adsorption on carbon nanotube bundles from molecular simulation. *Langmuir* **2004**, *20*, 10910−10918.

(7) Mao, Z. G.; Sinnott, S. B. Separation of organic molecular mixtures in carbon nanotubes and bundles: Molecular dynamics simulations/ *J. Phys. Chem. B* **2001**, *105*, 6916−6924.

(8) Jiang, J. W.; Sandler, S. I.; Schenk, M.; Smit, B. Adsorption and separation of linear and branched alkanes on carbon nanotube bundles from configurational-bias Monte Carlo simulation. *Phys. Rev. B: Condens. Matter* **2005**, *72*, 045447.

(9) Power, T. D.; Skoulidas, A. I.; Sholl, D. S. Can Chiral Single Walled Carbon Nanotubes Be Used as Enantiospecific Adsorbents? *J. Am. Chem. Soc.* **2002**, *124*, 1858−1859.

(10) Gu, C.; Gao, G. H.; Yu, Y. X.; Nitta, T. Simulation for separation of hydrogen and carbon monoxide by adsorption on single-walled carbon nanotubes. *Fluid Phase Equilib.* **2002**, *194*, 297−307.

(11) Challa, S. R.; Sholl, D. S.; Johnson, J. K. Adsorption and separation of hydrogen isotopes in carbon nanotubes: Multicomponent grand canonical Monte Carlo simulations. *J. Chem. Phys.* **2002**, *116*, 814−824.

(12) Chen, H.; Sholl, D. S. Predictions of selectivity and flux for CH_4/H_2 separations using single walled carbon nanotubes as membranes. *J. Membr. Sci.* **2006**, *269*, 152−160.

(13) Chen, H. B.; Sholl, D. S. Rapid diffusion of CH_4/H_2 mixtures in single-walk carbon nanotubes. *J. Am. Chem. Soc*. **2004**, *126*, 7778−7779.

(14) Skoulidas, A. I.; Ackerman, D. M.; Johnson, J. K.; Sholl, D. S. Rapid transport of gases in carbon nanotubes. *Phys. Rev. Lett.* **2002**, *89*, 185901.

(15) Skoulidas, A. I.; Sholl, D. S.; Johnson, J. K. Adsorption and Diffusion of Carbon Dioxide and Nitrogen through Single-Walled Carbon Nanotube Membranes. *J. Chem. Phys.* **2006**, *124*, 054708.

(16) Ackerman, D. M.; Skoulidas, A. I.; Sholl, D. S.; Johnson, J. K. Diffusivities of Ar and Ne in carbon nanotubes. *Mol. Simul.* **2003**, *29*, 677−684.

(17) Bhatia, S. K.; Chen, H. B.; Sholl, D. S. Comparisons of diffusive and viscous contributions to transport coefficients of light gases in single-walled carbon nanotubes. *Mol. Simul.* **2005**, *31*, 643−649.

(18) Chen, H.; Johnson, J. K.; Sholl, D. S. Transport of Gases is Rapid in Carbon Nanotubes. *J. Phys. Chem. B* **2006**, *110*, 1971−1975.

(19) Mao, Z. G.; Sinnott, S. B. A computational study of molecular diffusion and dynamic flow through carbon nanotubes. *J. Phys. Chem. B* **2000**, *104*, 4618−4624.

(20) Mao, Z. G.; Sinnott, S. B. Predictions of a spiral diffusion path for nonspherical organic molecules in carbon nanotubes. *Phys. Rev. Lett.* **2002**, *89*, 278301.

(21) Lee, K. H.; Sinnott, S. B. Computational studies of nonequilibrium molecular transport through carbon nanotubes. *J. Phys. Chem. B* **2004**, *108*, 9861−9870.

(22) Lee, K. H.; Sinnott, S. B. Equilibrium and nonequilibrium transport of oxygen in carbon nanotubes. *Nano Lett.* **2005**, *5*, 793−798.

(23) Arora, G.; Wagner, N. J.; Sandler, S. I. Adsorption and Diffusion of Molecular Nitrogen in Single Wall Carbon Nanotubes. *Langmuir* **2004**, *20*, 6268−6277.

(24) Nguyen, T. X.; Bhatia, S. K. Probing the pore wall structure of nanoporous carbons using adsorption. *Langmuir* **2004**, *20*, 3532−3535.

(25) Düren, T.; Jakobtorweihen, S.; Keil, F. J.; Seaton, N. A. Grand canonical molecular dynamics simulations of transport diffusion in geometrically heterogeneous pores. *Phys. Chem. Chem. Phys.* **2003**, *5*, 369−375.

(26) Düren, T.; Keil, F. J. Molecular modeling of adsorption in carbon nanotubes. *Chem. Eng. Technol.* **2001**, *24*, 698−702.

(27) Düren, T.; Keil, F. J.; Seaton, N. A. Composition dependent transport diffusion coefficients of CH_4/CF_4 mixtures in carbon nanotubes by nonequilibrium molecular dynamics simulations. *Chem. Eng. Sci.* **2002**, *57*, 1343−1354.

(28) Duren, T.; Keil, F. J.; Seaton, N. A. Molecular simulation of adsorption and transport diffusion of model fluids in carbon nanotubes. *Mol. Phys.* **2002**, *100*, 3741−3751.

(29) Heyden, A.; Duren, T.; Keil, F. J. Study of molecular shape and nonideality effects on mixture adsorption isotherms of small molecules in carbon nanotubes: A grand canonical Monte Carlo simulation study. *Chem. Eng. Sci.* **2002**, *57*, 2439−2448.

(30) Jakobtorweihen, S.; Verbeek, M. G.; Lowe, C. P.; Keil, F. J.; Smit, B. Understanding the Loading Dependence of Self-Diffusion in Carbon Nanotubes. *Phys. Rev. Lett.* **2005**, *95*, 044501.

(31) Vieira-Linhares, A. M.; Seaton, N. A. Nonequilibrium molecular dynamics simulation of gas separation in a microporous carbon membrane. *Chem. Eng. Sci.* **2003**, *58*, 4129−4136.

(32) Garberoglio, G.; Vallauri, R. Single particle dynamics of molecular hydrogen in carbon nanotubes. *Phys. Lett. A* **2003**, *316*, 407−412.

(33) Garberoglio, G.; Vallauri, R. Space-dependent diffusion of hydrogen in carbon nanotubes. *J. Mol. Liq.* **2005**, *117*, 43−47.

(34) Efremenko, R.; Sheintuch, M. Enthalpy and entropy effects in hydrogen adsorption on carbon nanotubes. *Langmuir* **2005**, *21*, 6282−6288.

(35) Kaganov, I. V.; Sheintuch, M. Nonequilibrium molecular dynamics simulation of gas-mixtures transport in carbon-nanopore membranes. *Phys. Rev. E: Stat. Phys., Plasmas, Fluids, Relat. Interdiscip. Top.* **2003**, *68*, 046701.

(36) Zheng, J.; Lennon, E. M.; Tsao, H. K.; Sheng, Y. J.; Jiang, S. Y. Transport of a liquid water and methanol mixture through carbon nanotubes under a chemical potential gradient. *J. Chem. Phys.* **2005**, *122*, 214702.

(37) Sokhan, V. P.; Nicholson, D.; Quirke, N. Transport properties of nitrogen in single walled carbon nanotubes. *J. Chem. Phys.* **2004**, *120*, 3855−3863.

(38) Li, H. J.; Lu, W. G.; Li, J. J.; Bai, X. D.; Gu, C. Z. Multichannel Ballistic Transport in Multiwall Carbon Nanotubes. *Phys. Rev. Lett.* **2005**, *95*, 086601.

(39) Skoulidas, A. I.; Bowen, T. C.; Doelling, C. M.; Falconer, J. L.; Noble, R. D.; Sholl, D. S. Comparing atomistic simulations and experimental measurements for CH_4/CF_4 mixture permeation through silicalite membranes. *J. Membr. Sci.* **2003**, *227*, 123−136.

(40) Krishna, R. Problems and Pitfalls in the Use of the Fick Formulation for Intraparticle Diffusion. *Chem. Eng. Sci.* **1993**, *48*, 845−861.

(41) Krishna, R.; Wesselingh, J. A. The Maxwell−Stefan approach to mass transfer. *Chem. Eng. Sci.* **1997**, *52*, 861−911.

(42) Kapteijn, F.; Moulijn, J. A.; Krishna, R. The generalized Maxwell−Stefan model for diffusion in zeolites: sorbate molecules with different saturation loadings. *Chem. Eng. Sci.* **2000**, *55*, 2923−2930.

(43) Skoulidas, A. I.; Sholl, D. S.; Krishna, R. Correlation effects in diffusion of CH_4/CF_4 mixtures in MFI zeolite. A study linking MD simulations with the Maxwell−Stefan formulation. *Langmuir* **2003**, *19*, 7977−7988.

(44) Chempath, S.; Krishna, R.; Snurr, R. Q. Nonequilibrium MD simulations of difusion of binary mixtures containing short *n*-alkanes in faujasite. *J. Phys. Chem. B* **2004**, *108*, 13481−13491.

(45) Krishna, R.; van Baten, J. M. Diffusion of alkane mixtures in zeolites. Validating the Maxwell−Stefan formulation using MD simulations. *J. Phys. Chem. B* **2005**, *109*, 6386-6396.

(46) van Baten, J. M.; Krishna, R. Entropy effects in adsorption and diffusion of alkane isomers in mordenite: An investigation using CBMC and MD simulations. *Microporous Mesoporous Mater.* **2005**, *84*, 179−191.

(47) Krishna, R.; Van Baten, J. M. Influence of isotherm inflection on the diffusivities of C5−C8 linear alkanes in MFI zeolite. *Chem. Phys. Lett.* **2005**, *407*, 159−165.

(48) Skoulidas, A. I.; Sholl, D. S. Direct tests of the Darken approximation for molecular diffusion in zeolites using equilibrium molecular dynamics. *J. Phys. Chem. B* **2001**, *105*, 3151−3154.

(49) Kärger, J.; Vasenkov, S.; Auerbach, S. M. *Diffusion in zeolites*, Chapter 10. Handbook of Zeolite and Technology; Auerbach, S. M., Carrado, K. A., Dutta, P. K., Eds.; Marcel Dekker: New York, 2003.

(50) Dubbeldam, D.; Calero, S.; Vlugt, T. J. H.; Krishna, R.; Maesen, T. L. M.; Smit, B. United Atom Forcefield for Alkanes in Nanoporous Materials. *J. Phys. Chem. B* **2004**, *108*, 12301−12313.

(51) Steele, W. A. *The Interaction of Gases With Solid Surfaces*; Pergamon Press: Oxford, U.K., 1974.

(52) Buch, V. Path integral simulations of mixed para-D2 and ortho-D2 clusters: The orientational effects. *J. Chem. Phys.* **1994**, *100*, 7610−7629.

(53) Dubbeldam, D.; Calero, S.; Vlugt, T. J. H.; Krishna, R.; Maesen, T. L. M.; Beerdsen, E.; Smit, B. Force Field Parametrization through Fitting on Inflection Points in Isotherms. *Phys. Rev. Lett.* **2004**, *93*, 088302.

(54) Calero, S.; Dubbeldam, D.; Krishna, R.; Smit, B.; Vlugt, T. J. H.; Denayer, J. F. M.; Martens, J. A.; Maesen, T. L. M. Understanding the role of sodium during adsorption. A force field for alkanes in sodium exchanged faujasites. *J. Am. Chem. Soc.* **2004**, *126*, 11377−11386.

(55) Frenkel, D.; Smit, B. *Understanding molecular simulations: From algorithms to applications*; 2nd ed.; Academic Press: San Diego, CA, 2002.

(56) Skoulidas, A. I.; Sholl, D. S. Molecular Dynamics Simulations of Self, Corrected, and Transport Diffusivities of Light Gases in Four Silica Zeolites to Assess Influences of Pore Shape and Connectivity. *J. Phys. Chem. A* **2003**, *107*, 10132−10141.

(57) Krishna, R.; Paschek, D.; Baur, R. Modelling the occupancy dependence of diffusivities in zeolites. *Microporous Mesoporous Mater.* **2004**, *76*, 233−246.

(58) Reed, D. A.; Ehrlich, G. Surface diffusion, atomic jump rates and thermodynamics. *Surf. Sci.* **1981**, *102*, 588−609.

(59) Krishna, R.; Paschek, D. Self-diffusivities in multicomponent mixtures in zeolites. *Phys. Chem. Chem. Phys.* **2002**, *4*, 1891−1898.

(60) Clark, L. A.; Gupta, A.; Snurr, R. Q. Siting and segregation effects of simple molecules in zeolites MFI, MOR, and BOG. *J. Phys. Chem. B* **1998**, *102*, 6720−6731.

(61) Krishna, R.; Van Baten, J. M. The Darken relation for multicomponent diffusion in liquid mixtures of linear alkanes. An investigation using molecular dynamics (MD) simulations. *Ind. Eng. Chem. Res.* **2005**, *44*, 6939−6947.

(62) Greiner-Schmid, A.; Wappmann, S.; Has, M.; Lüdemann, H. D. Self-diffusion in the compressed fluid lower alkanes: Methane, ethane, and propane. *J. Chem. Phys.* **1991**, *94*, 5643−5649.

(63) Krishna, R.; Smit, B.; Calero, S. Entropy effects during sorption of alkanes in zeolites. *Chem. Soc. Rev.* **2002**, *31*, 185−194.

Received for review October 10, 2005
Revised manuscript received December 7, 2005
Accepted January 18, 2006

IE051126D

Describing binary mixture diffusion in carbon nanotubes with the Maxwell-Stefan equations. An investigation using molecular dynamics simulations

R. Krishna and J.M. van Baten
University of Amsterdam

- Contains data on Δ_{ij}, $D_{i,self}$, $Đ_i$, $Đ_{ii}$ for all the campaigns listed in Table 1 of the manuscript
- The symbols represent the MD simulated data
- The continuous solid lines represent calculations based on the Maxwell-Stefan theory, Eqs (14) and (15), and using pure component parameters listed in Table 4.

CNT (20,0)

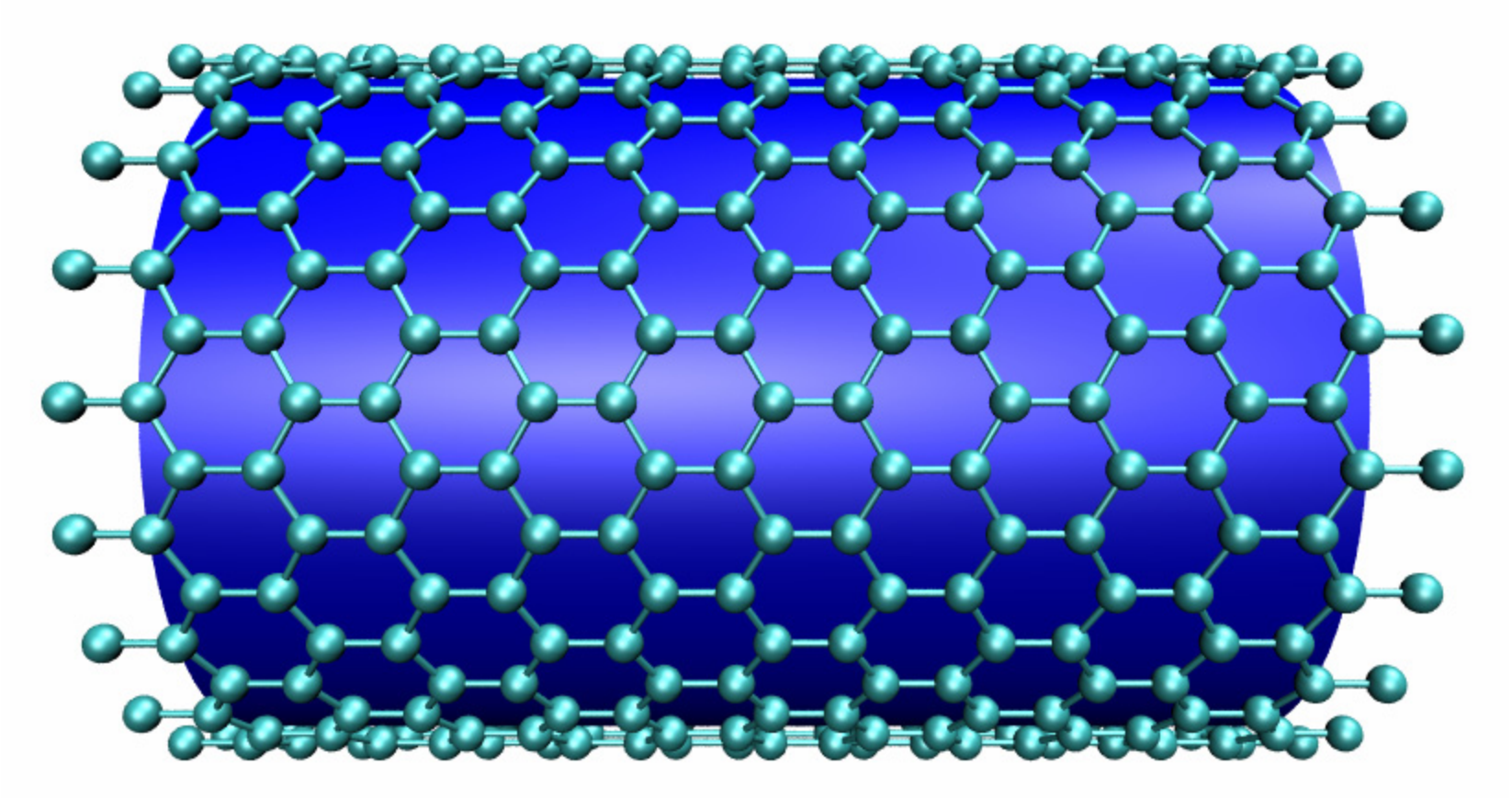

CNT (20,0); pure C1 adsorption, snapshots, 300 K

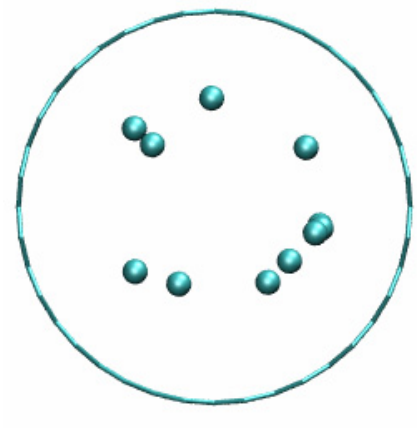

50 kPa

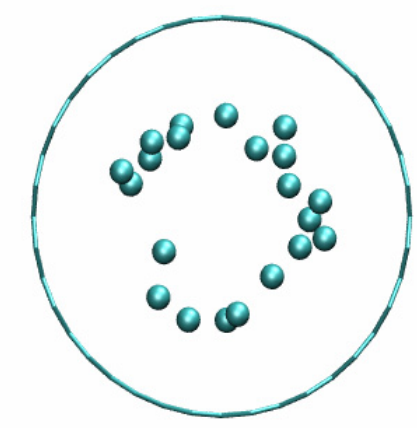

100 kPa

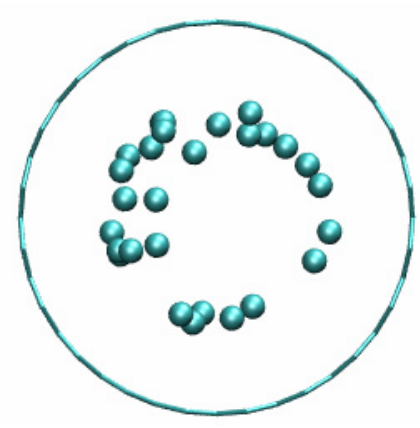

200 kPa

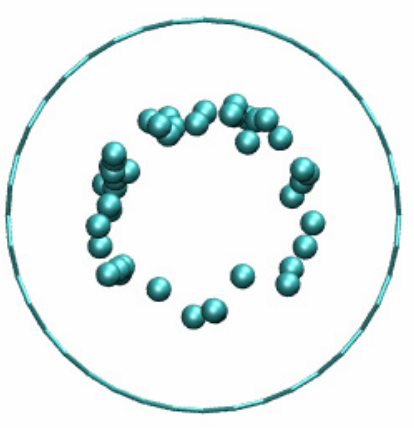

240 kPa

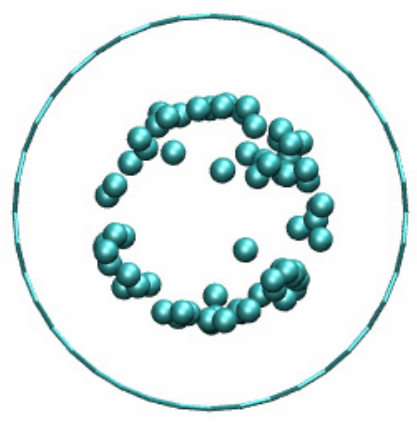

500 kPa

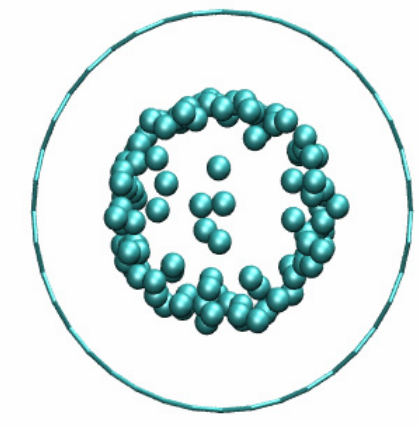

1000 kPa

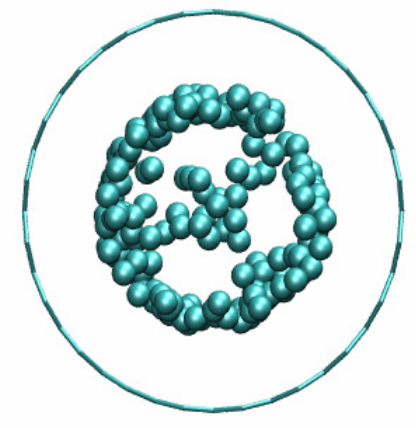

10000 kPa

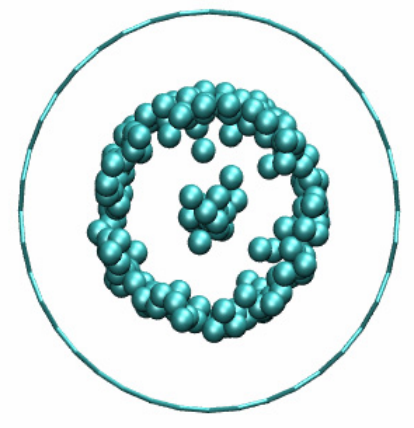

100000 kPa

CNT (20,0); pure C2 adsorption, snapshots, 300 K

5 kPa

6 kPa

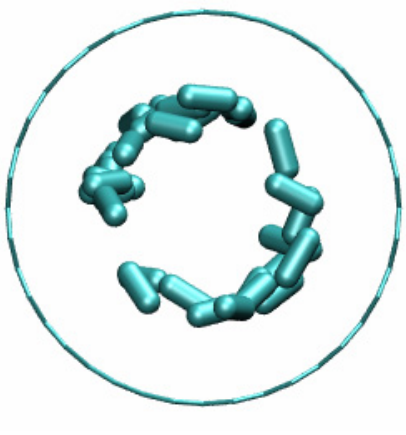

14 kPa

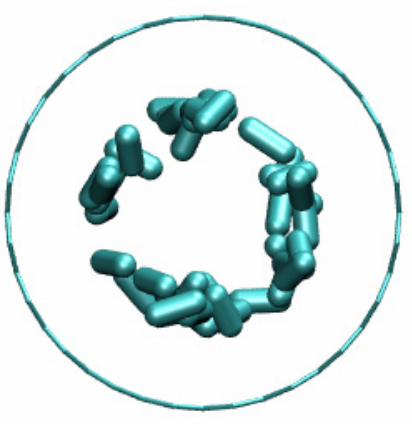

20 kPa

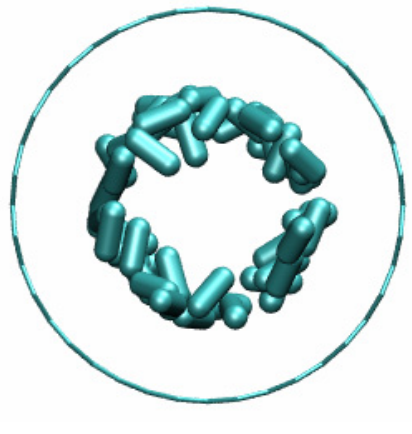

25 kPa

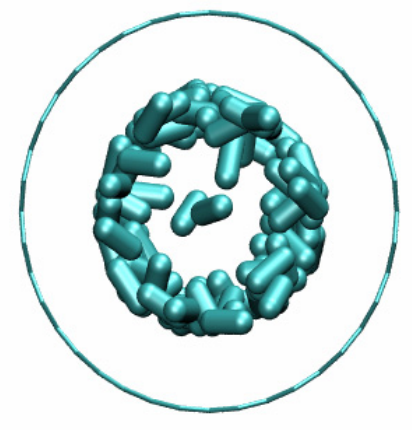

100 kPa

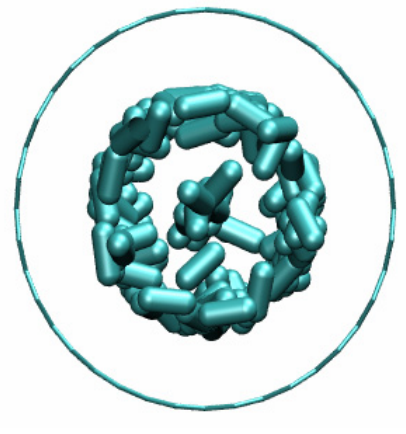

1000 kPa

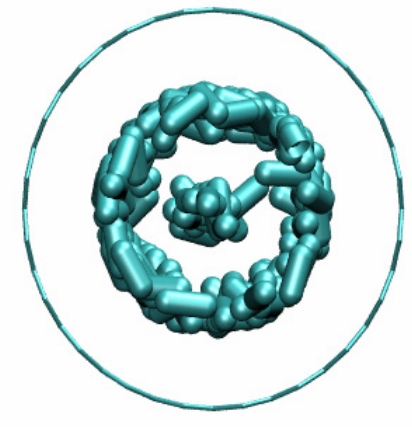

10000 kPa

CNT (20,0); C1, C2, and C1-C2 mixture, 300 K

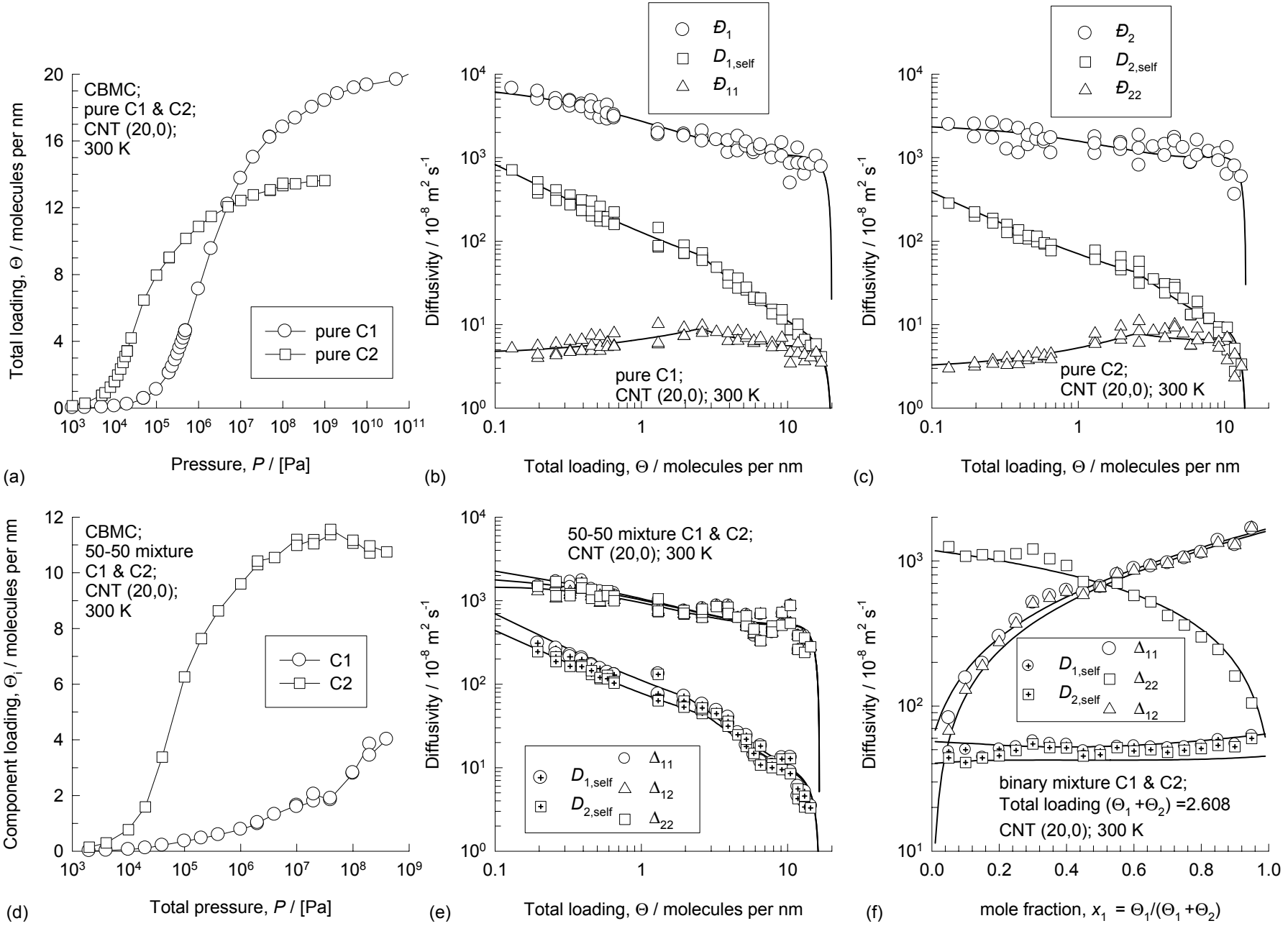

CNT (20,0) vs Fluid; C1, C2, and C1-C2 mixture, 300 K

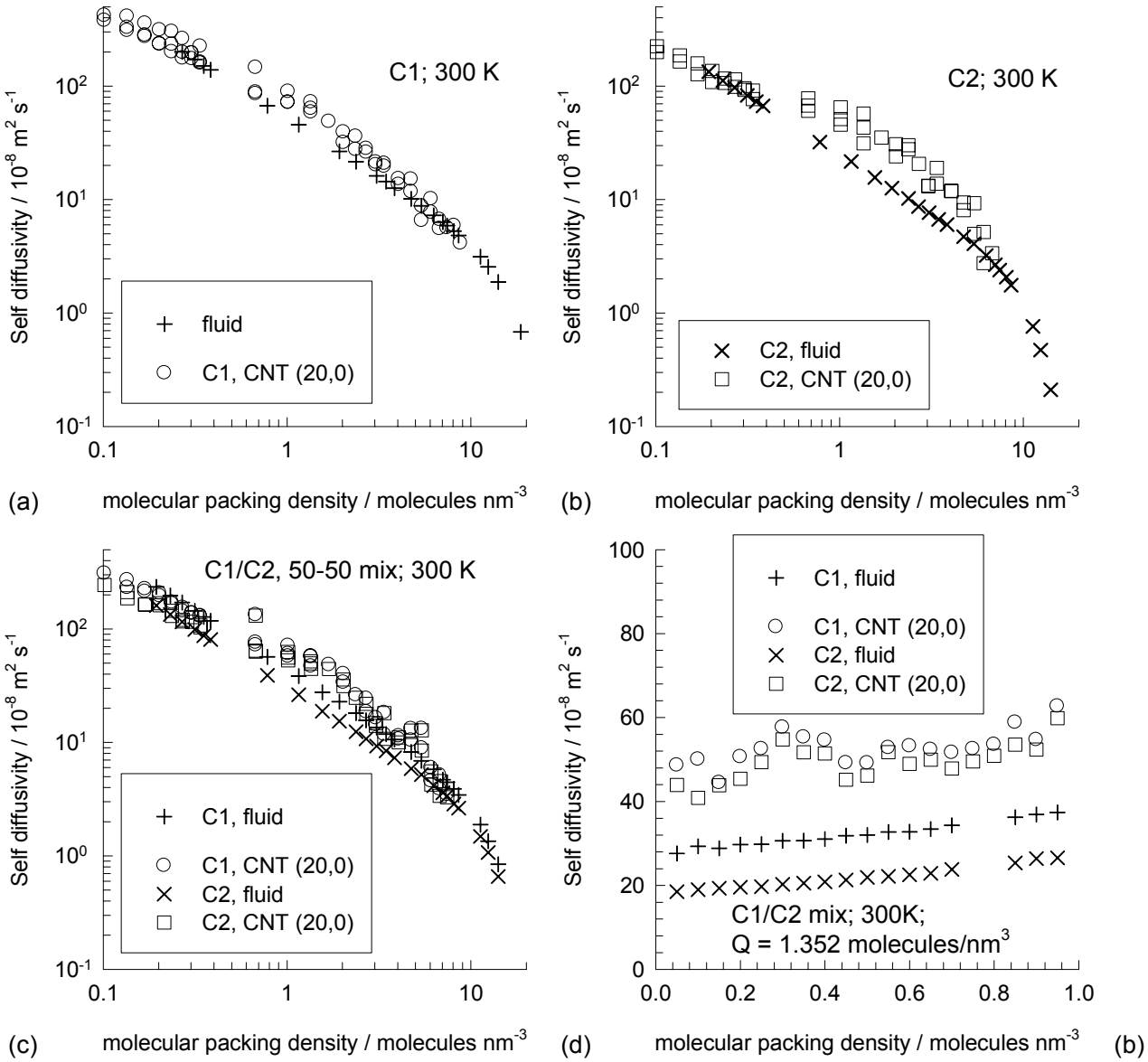

CNT (20,0); C1, C3, and C1-C3 mixture, 300 K

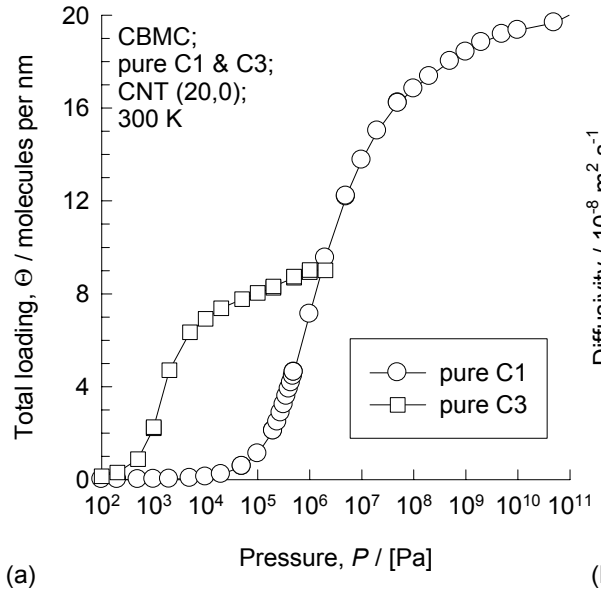

(a)

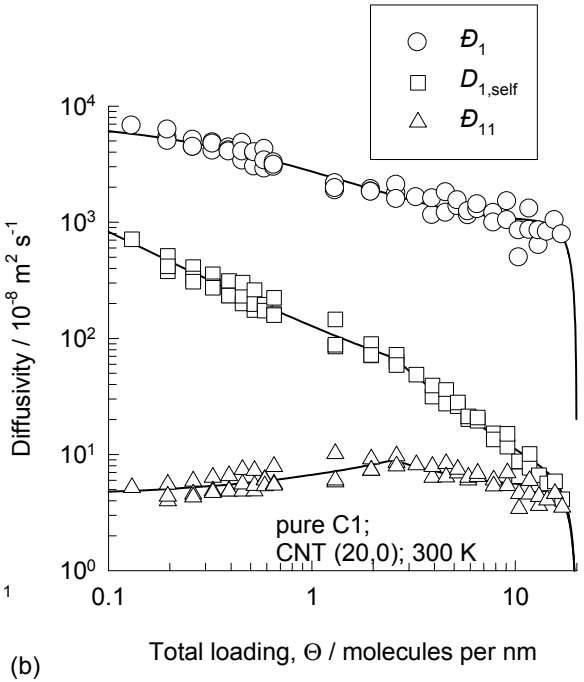

(b)

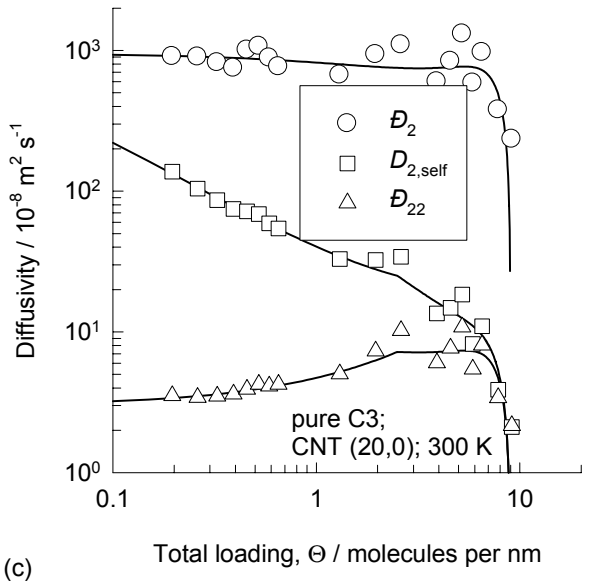

(c)

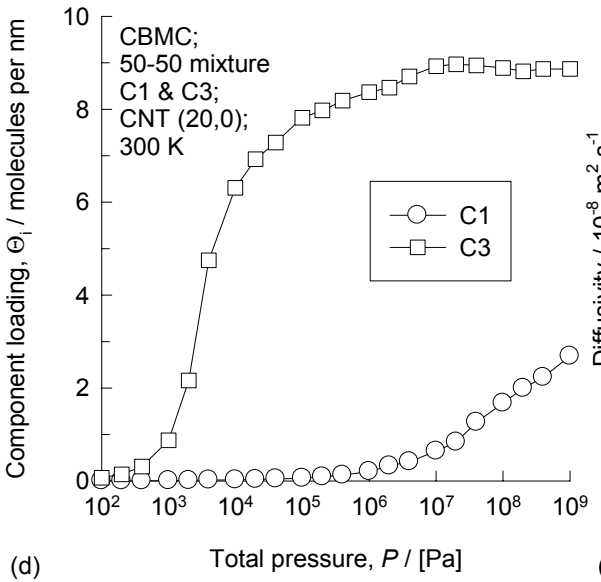

(d)

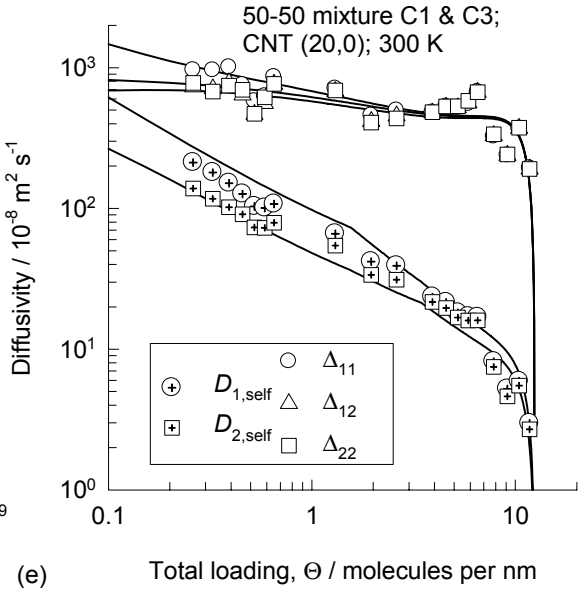

(e)

CNT (20,0) vs Fluid; C1, C3, and C1-C3 mixture, 300 K

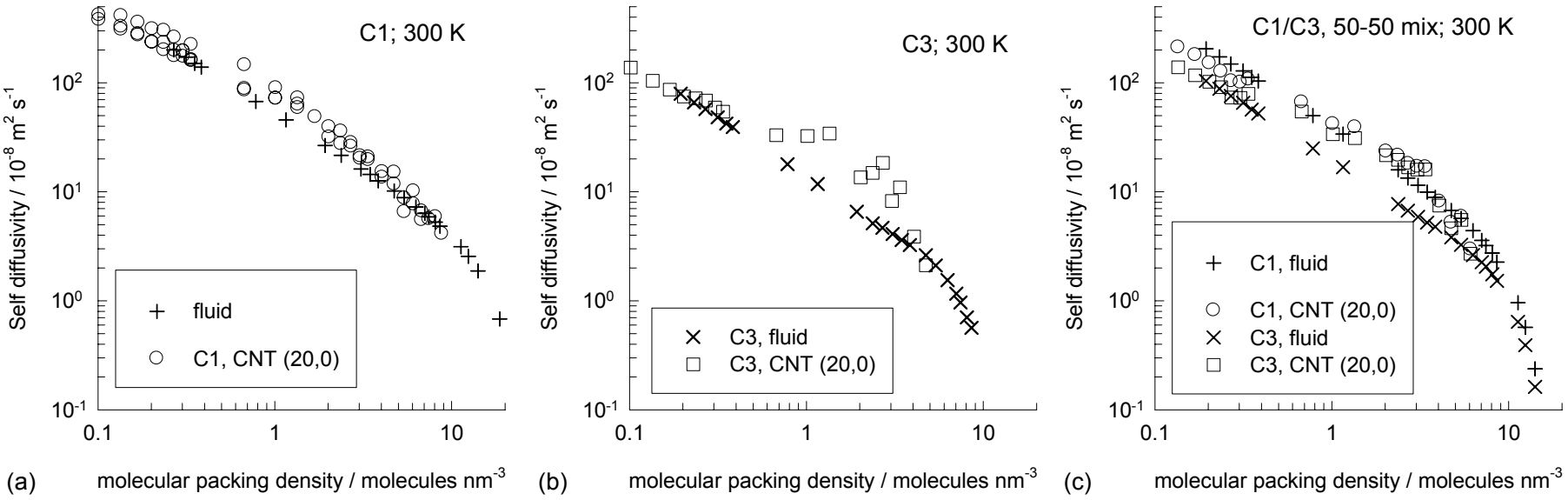

CNT (20,0); C1, nC4, and C1-nC4 mixture, 300 K

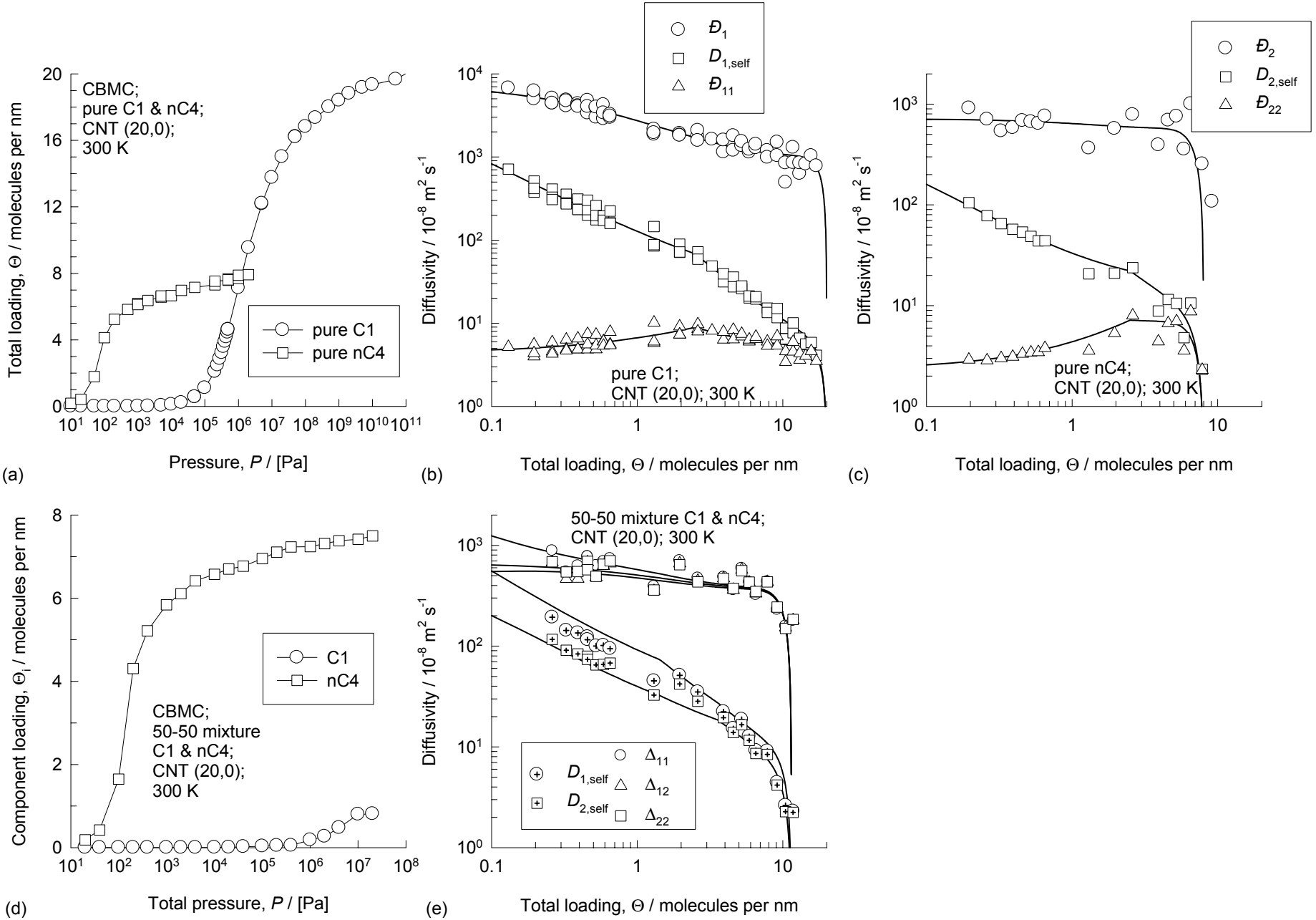

CNT (20,0) vs Fluid; C1, nC4, and C1-nC4 mixture, 300 K

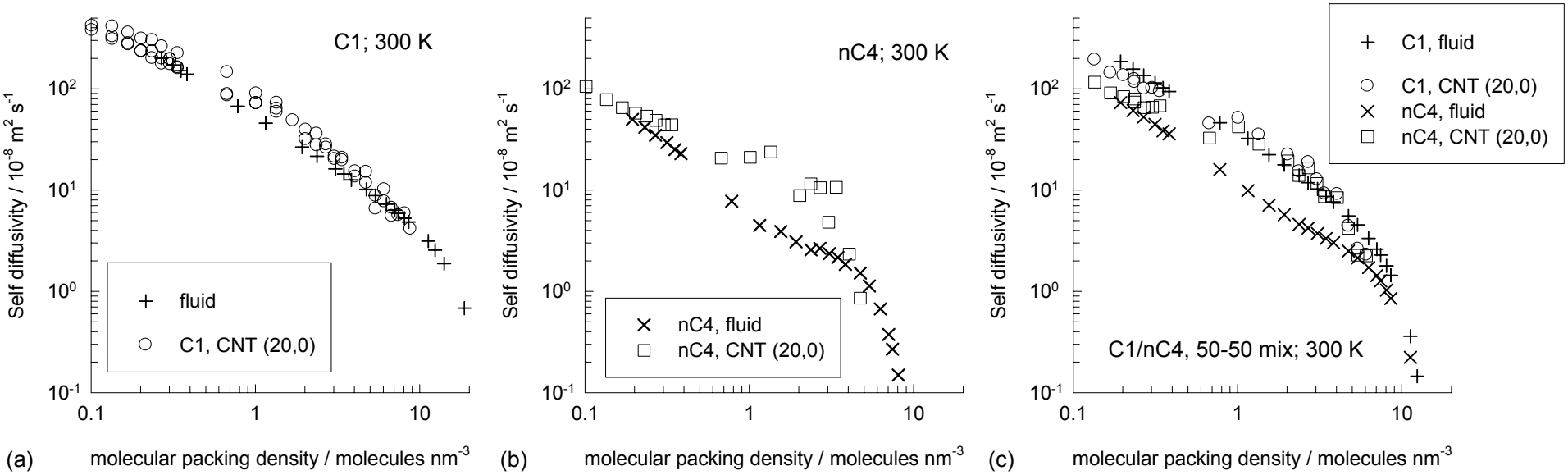

CNT (20,0); C1, iC4, and C1-iC4 mixture, 300 K

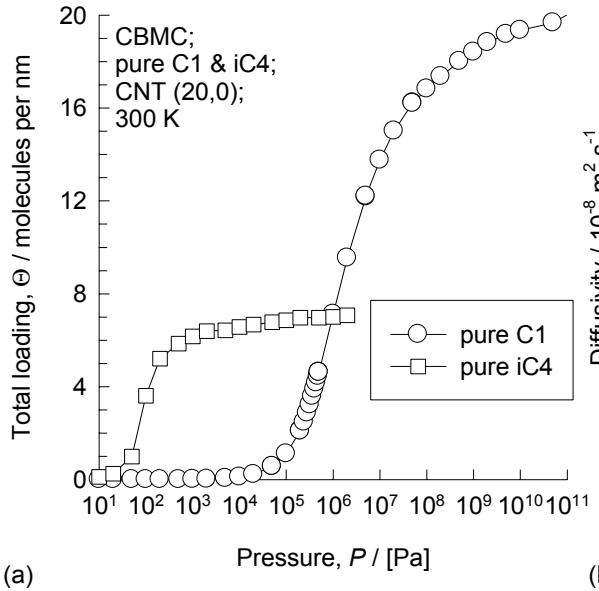

(a)

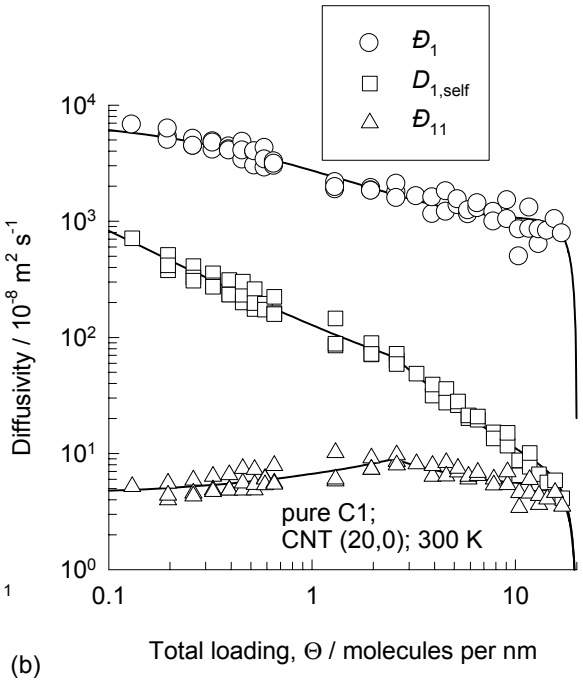

(b)

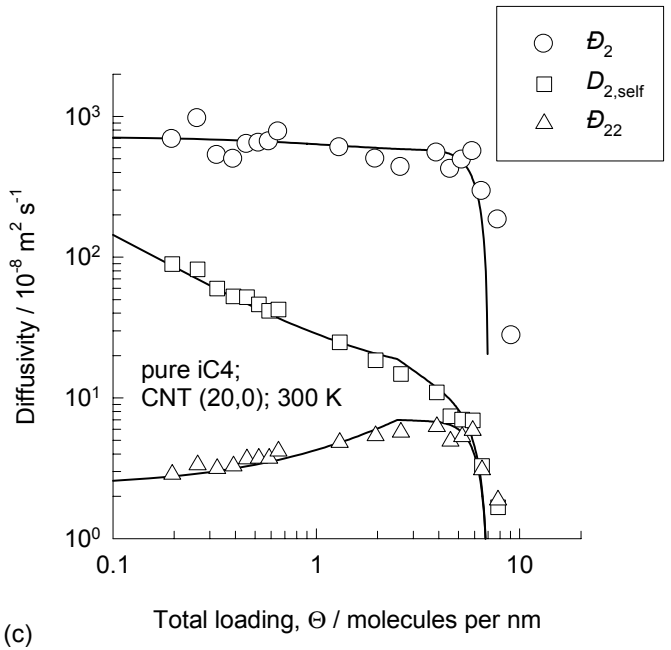

(c)

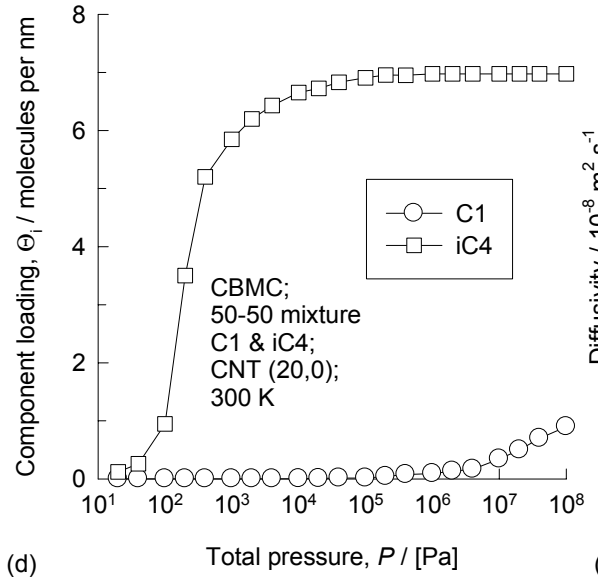

(d)

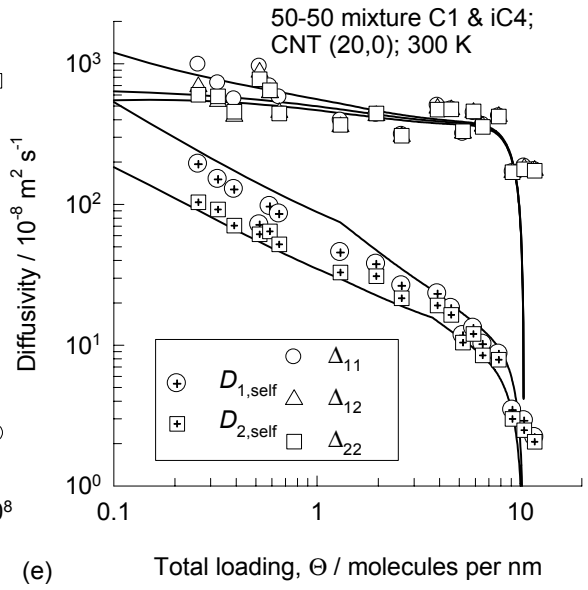

(e)

CNT (20,0) vs Fluid; C1, iC4, and C1-iC4 mixture, 300 K

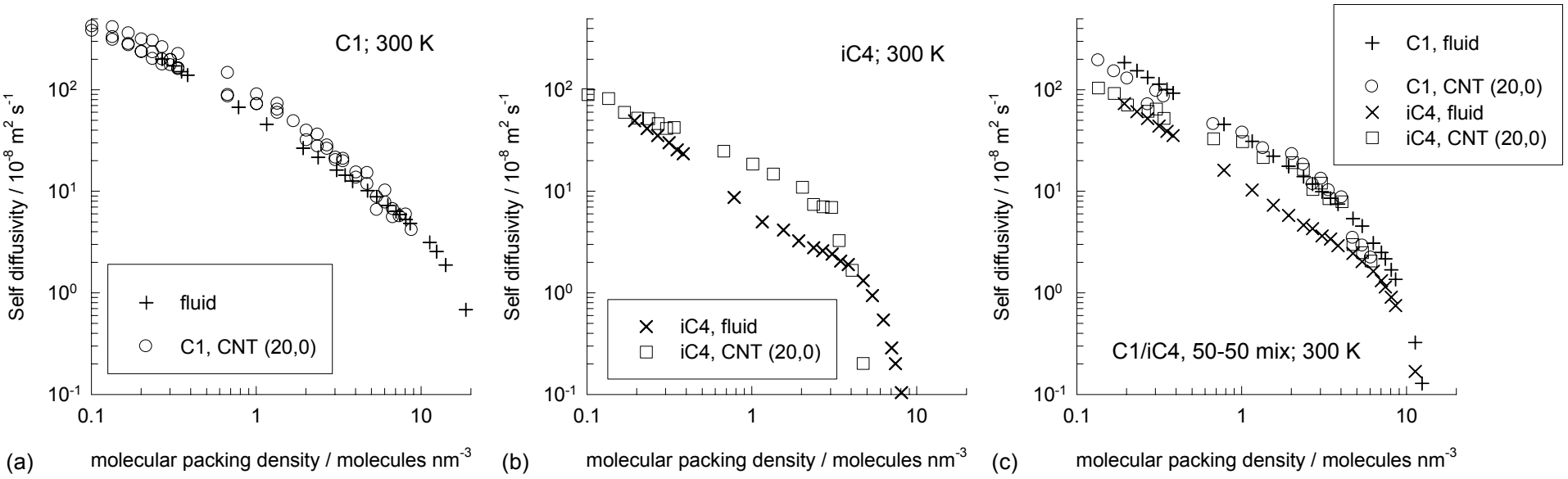

CNT (10,10)

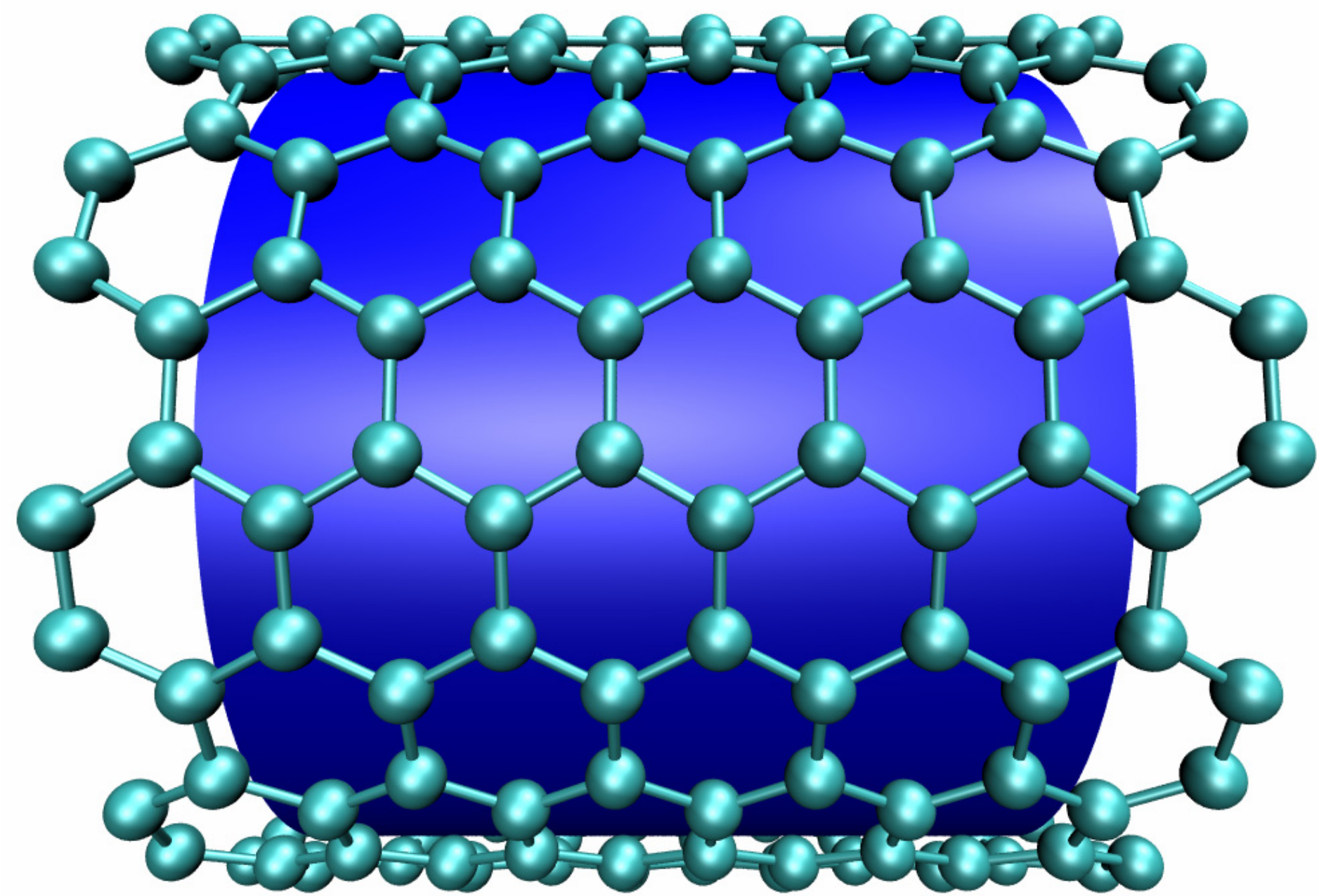

CNT (10,10); pure C1 adsorption, snapshots, 300 K

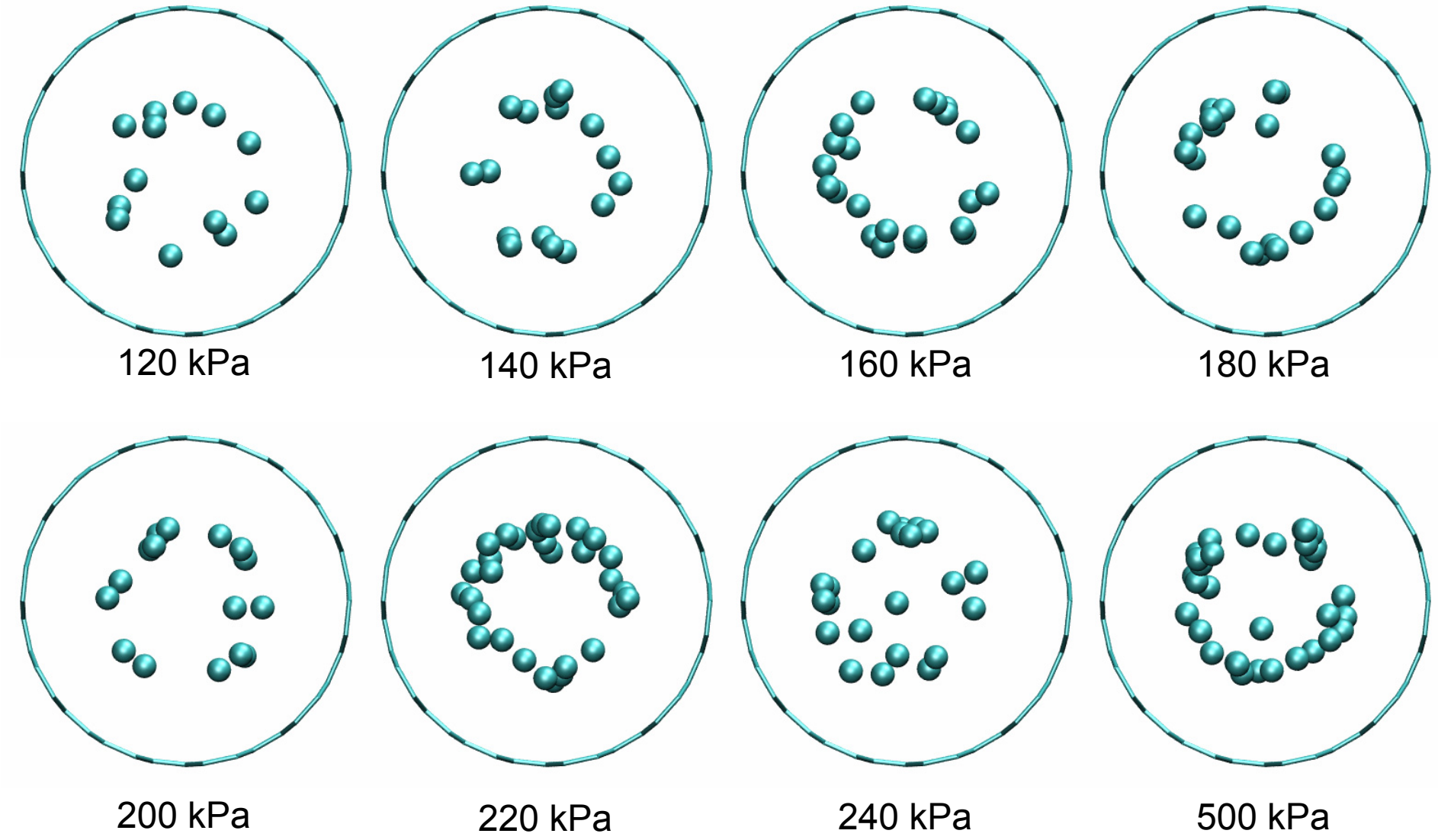

CNT (10,10); pure H2 adsorption, snapshots, 300 K

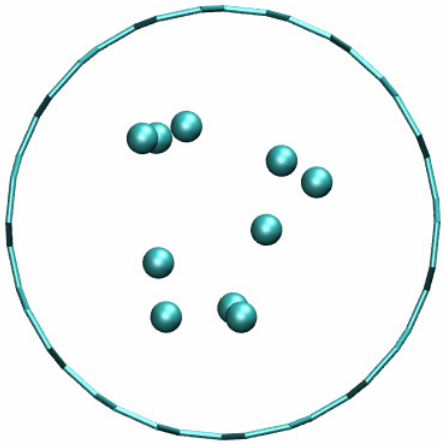

4400 kPa

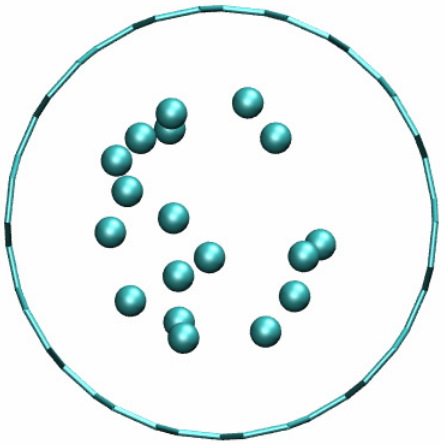

4800 kPa

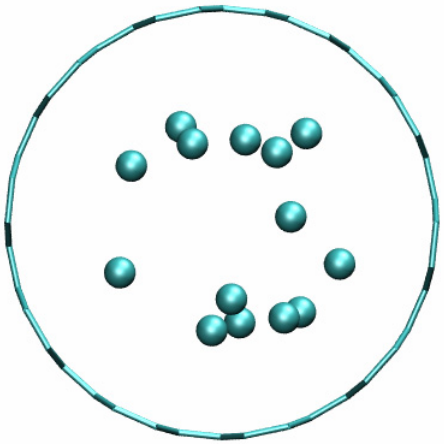

5000 kPa

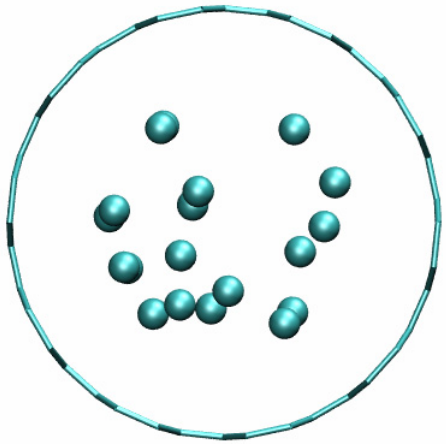

5200 kPa

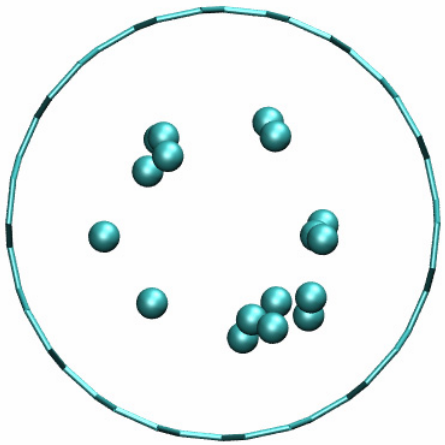

5600 kPa

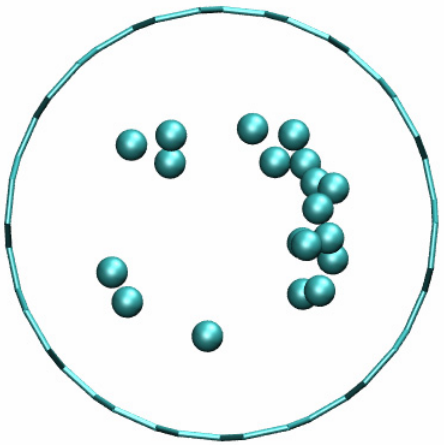

6000 kPa

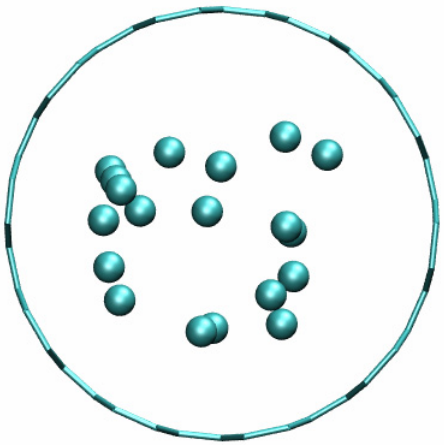

6400 kPa

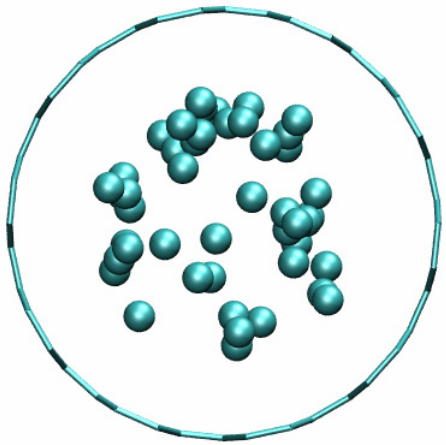

15000 kPa

CNT (10,10); C1, H2, and C1-H2 mixture, 300 K

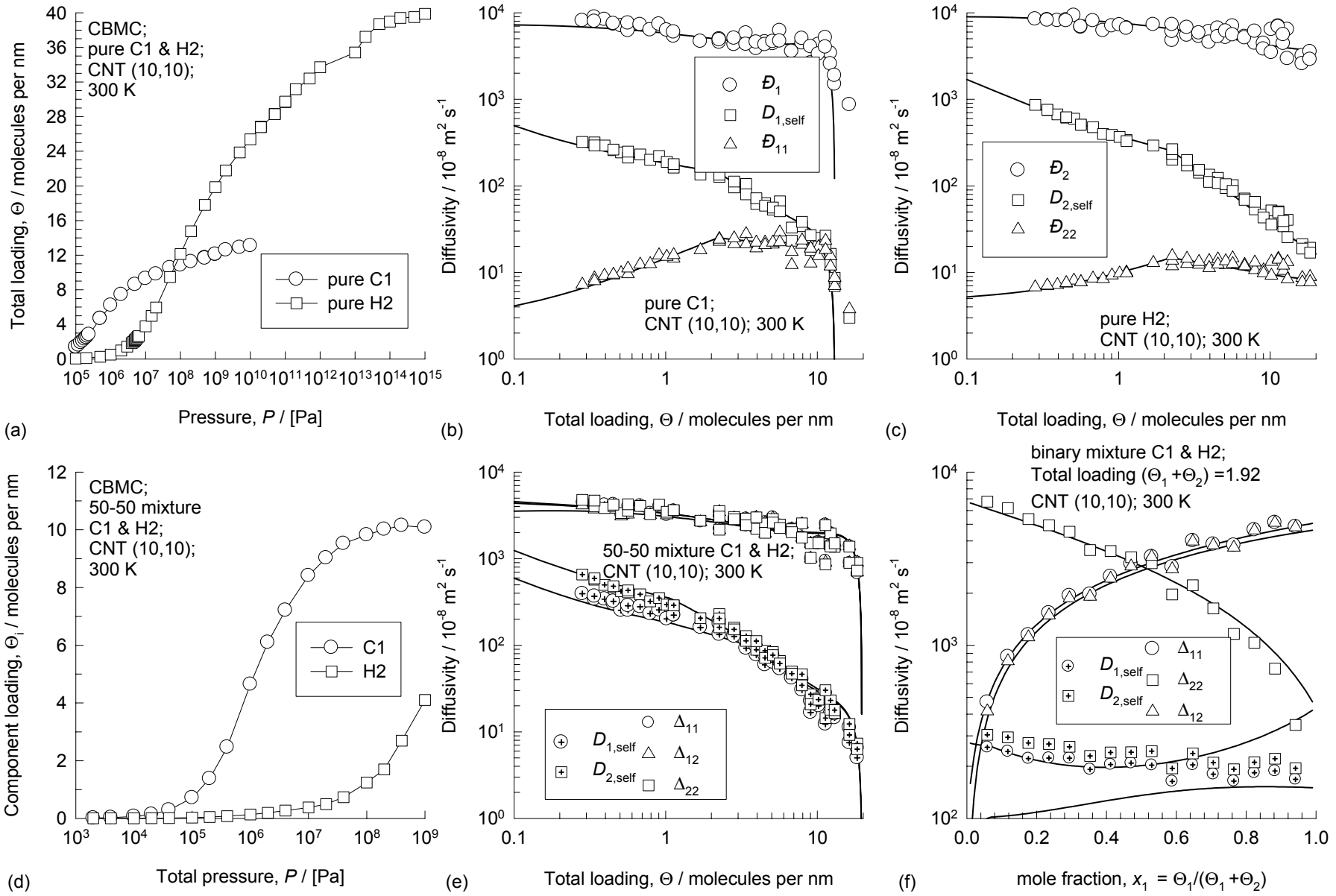

CNT (10,10) vs Fluid; C1, H2, and C1-H2 mixture, 300 K